A mathematical model of tumor–immune interactions

Mark Robertson-Tessi [a,*], Ardith El-Kareh [b], Alain Goriely [c]

[a] *Program in Applied Mathematics, University of Arizona, Tucson, AZ 85721, United States*
[b] *ARL-Microcirculation Division, University of Arizona, Tucson, AZ 85724, United States*
[c] *Oxford Center for Collaborative Applied Mathematics, Mathematical Institute, Oxford OX2 6HA, UK*

ABSTRACT

A mathematical model of the interactions between a growing tumor and the immune system is presented. The equations and parameters of the model are based on experimental and clinical results from published studies. The model includes the primary cell populations involved in effector T-cell mediated tumor killing: regulatory T cells, helper T cells, and dendritic cells. A key feature is the inclusion of multiple mechanisms of immunosuppression through the main cytokines and growth factors mediating the interactions between the cell populations. Decreased access of effector cells to the tumor interior with increasing tumor size is accounted for. The model is applied to tumors with different growth rates and antigenicities to gauge the relative importance of various immunosuppressive mechanisms. The most important factors leading to tumor escape are TGF-β-induced immunosuppression, conversion of helper T cells into regulatory T cells, and the limitation of immune cell access to the full tumor at large tumor sizes. The results suggest that for a given tumor growth rate, there is an optimal antigenicity maximizing the response of the immune system. Further increases in antigenicity result in increased immunosuppression, and therefore a decrease in tumor killing rate. This result may have implications for immunotherapies which modulate the effective antigenicity. Simulation of dendritic cell therapy with the model suggests that for some tumors, there is an optimal dose of transfused dendritic cells.

© 2011 Elsevier Ltd. All rights reserved.

1. Introduction and motivation

Understanding the interplay between a growing tumor and the host's immune system is fundamental for optimizing current treatments and proposing new ones. Despite much research into these tumor–immune interactions (Dunn et al., 2002; Villunger and Strasser, 1999), there are many open questions in the field and quantitative theories are relatively few. Although the immune system is known to play a role in the prevention and removal of some tumors, it appears to be incapable of fighting others (Vaage, 1971). Recent research suggests that immunosuppression is a significant obstacle that the immune system faces when fighting a tumor (Chouaib et al., 1997). Since there are many forms of immunosuppression acting at different levels of the immune system, it is important to quantify the effect of each suppressive element at each stage of tumor growth.

Mathematical modeling has been used in conjunction with experimental and clinical results to explore the significance of tumor–immune interactions. Previous work has included models of T cells with interleukin-2 (IL-2) (Kirschner and Panetta, 1998),

transforming growth factor beta (TGF-β) (Arciero et al., 2004), regulatory T cells (Tregs) (Leon et al., 2007), and natural killer cells (de Pillis et al., 2005).

The mathematical model presented in this paper examines the T-cell response to a tumor. Several new features are included in the model. Multiple suppressive elements are modeled, so that their respective effect can be quantified at different stages of tumor growth. The growth law of the tumor is modeled as a hybrid between exponential and power law growth. Immune cell access to the interior of a large tumor is limited, based on perfusion data. Helper T cells are also included in the model, since they affect the dynamics of the immune response. In addition, helper T cells can be converted into regulatory T cells by TGF-β, recently found to be a significant factor leading to creation of these cells (Liu et al., 2007b). All of the parameters were estimated from experimental and clinical data. Although these parameters necessarily come from different systems, using realistic parameter values ensures that the model operates within a biologically reasonable regime.

The paper is organized as follows: Section 2 briefly outlines the biological processes involved in mounting a T-cell immune response to a tumor. The mathematical model is presented in Section 3, and the derivation of parameters is given in Section 4. Analysis of the model and an application of immunotherapy are described in Section 5. Conclusions and ideas for further development of this model are given in Section 6.

---

*Corresponding author. Current address: Integrated Mathematical Oncology, Moffitt Cancer Center, Tampa, FL 33612, United States. Tel.: +1 813 745 6818.
E-mail address: mark.robertsontessi@moffitt.org (M. Robertson-Tessi).

2. Tumor–immune interactions

Many murine and *in vitro* studies have shown that tumor cells can be killed by immune system cells (Hellstrom and Hellstrom, 1974; Boon et al., 1994). Tumors present antigens, and usually T cells capable of recognizing that antigen exist in the body. It is likely that in humans some tumors may be removed by the immune system before they are detected. Of course, these instances are not recorded, since the tumor never becomes symptomatic. In murine studies, though, spontaneous tumor regression and tumor immunity have been demonstrated (Boon et al., 1994). Furthermore, immunodeficient mice have been shown to have increased incidence of cancers (Dunn et al., 2006), and human patients taking immunosuppressive agents also show increased susceptibility to many cancer types (Wimmer et al., 2007), suggesting that the immune system plays a role in the spontaneous removal of some small tumors.

However, the prevalence of cancer indicates that the immune system does not have a strong enough effect against all forms of the disease. This failure of the immune system is thought to occur for two reasons. The first is an insufficient immune response due to the tumor being poorly antigenic. This is described by Curiel as "too little of a good thing" (Curiel, 2007). Cytotoxic T cells are not sufficiently activated by the tumor, and therefore the response is minimal. The second cause for failure is "too much of a bad thing," in which immunosuppressive factors dampen an otherwise capable immune system. Over the past few decades, the importance of the second paradigm has become clear; immunosuppression is likely to be a significant factor when cancer is present in the host.

Although other immune cells play a role in fighting cancer, T cells have been suggested as one of the principal methods that the body uses to combat a tumor (Hellstrom and Hellstrom, 1991; Rosenberg et al., 1986). As the tumor grows, it provokes an immune response from the T cells in the host. The strength of this response depends on the tumor's antigenicity, which describes how much antigen a tumor presents, and also how sensitive the immune system is to this antigen. At the same time, immunosuppressive factors secreted by the tumor and invoked by the host can act to limit the immune response.

In the cases where a tumor reaches a clinical size on the order of 10^9–10^{11} cells, there are several mechanisms by which the tumor may have escaped the immune response. One possibility is that the antigens presented by the tumor are not strong or prevalent enough to elicit an immune response. In this case, the tumor is not recognized as a significant threat by the immune system. Another possibility is that antigen may be present in sufficient strength, but the immunosuppressive elements may be reducing the efficacy of the immune system. Research has shown that some murine tumors which have grown without check can be removed by the immune system after certain suppressive factors are blocked (Gorelik and Flavell, 2001; Viehl et al., 2006). This suggests that the immune system has the capability to fight the tumor, but that the suppressive effects prevent proper action of the T cells on the tumor.

In a simplified model of an immune response to a tumor, excluding any immunosuppression, the system can be seen as a predator–prey system. The T-cell response would fall into three categories. If the antigenicity is high enough, the tumor will provoke a large immune response, and the T cells will fully remove the tumor. If the antigenicity is very low, then the T-cell reaction will be minimal. The immune system may slow down the tumor growth rate, but the tumor will continue to grow without bound. At a moderate antigenicity, there may exist an equilibrium state, where the tumor growth rate and the immune system killing rate balance each other.

The addition of immunosuppression adds a complex negative feedback loop to the activation of the immune system. The tumor not only provokes an immune response as described above, but also promotes suppression of the immune system, which will diminish the T-cell response. There are a number of mechanisms for this suppression; the literature suggests that the significant sources of T-cell immunosuppression are Tregs (Viehl et al., 2006; Frumento et al., 2006), TGF-β (Gorelik and Flavell, 2001; Kobie and Akporiaye, 2003; Wojtowicz-Praga, 2003), and interleukin-10 (IL-10) (Avradopoulos et al., 1997; Hsieh et al., 2000). These immunosuppressive elements act in different ways on the system, and have different levels of activity at different stages of tumor growth. The model of these interactions is presented in the following section.

3. A mathematical model

3.1. Variables

Since the interactions between the immune system and a tumor are highly complex, a full model which includes all the significant cell types and signaling molecules is unrealistic. However, if the model is too simple, the results will be trivial and will fail to produce the complex dynamics observed in experimental and clinical settings.

In selecting the variables to consider in this model, several principles were used as a guide. First, the values of the parameters appearing in an equation must be obtainable from experimental data which allows for a reasonable estimation of a biologically appropriate range. Second, enough cell types and interactions must be included to capture the short time scale dynamics of T-cell proliferation observed in experiments. The activation and proliferation of T cells is subject to competition between the different T-cell types, and involves several phases which have different characteristic time scales. Third, the immune system must respond naturally in the absence of tumor-induced suppressive terms, as opposed to only acting reasonably when these suppressive effects are applied.

The model presented here uses 12 biological variables: nine cell types and three cytokines. Naturally, tumor cells are included, and are denoted by the variable $T(t)$, where t stands for time in days. The heterogeneity of the interactions between tumor cells and the immune system is an important effect that is neglected in this model due to a lack of specific experimental data. Therefore, in the model all tumor cells behave in the same way.

While there is no explicit spatial component to the model at this time, tumor vasculature is accounted for by its action on tumor growth rate and immune system access. The model assumes that the tumor is perfused from the outside. Therefore, immune system cells will only be able to interact with a layer of the tumor, once the tumor becomes large compared to the perfusion depth.

In order to investigate the effects of the T-cell response, the model must include CD8$^+$ effector T cells, which directly kill the tumor cells. In addition, CD4$^+$ CD25$^+$ Foxp3$^+$ regulatory T cells are included in order to account for immunosuppression, since they produce suppressive cytokines and also act directly to reduce effector T-cell killing rates.

Stimulation of T cells occurs in the lymph nodes, and begins when antigen-presenting cells (APCs) bearing tumor antigens interact with the T cells. In this model, dendritic cells are the chosen APCs, since they are the primary mechanism for T-cell activation (Roitt and Delves, 2001).

A third population of T cells, CD4$^+$ helper T cells, is included to assist with cytokine production and dendritic cell licensing.

The inclusion of helper T cells as a distinct population is necessary for two reasons. First, the helper cells license the dendritic cells, which prevents an unrealistically rapid development of effector T cells. Second, the helper cells are converted to Tregs by TGF-β, a key immunosuppressive mechanism observed in experiments (Liu et al., 2007b).

All three types of T cells are specific to the tumor antigen, and comprise a small fraction of the total T-cell repertoire within a host. Each of the three T-cell populations are broken into three subpopulations. The memory T cell population (M_E, M_H, and M_R, all assumed to be constant) is a pool of T-cell precursors, which are activated by dendritic cells. There is a short-lived activation phase ($A_E(t)$, $A_H(t)$, and $A_R(t)$) where T-cell proliferation occurs. The fully functional T-cell phase ($E(t)$, $H(t)$, and $R(t)$) consists of the cells that kill the tumor cells, produce cytokines, and suppress the immune response. These subpopulations capture the different time scales of the cellular phases, and contribute three constants and six variables to the model.

The dendritic cell population has two subpopulations. The unlicensed state, $U(t)$, is a mature dendritic cell that collects antigen from the tumor, and then interacts with helper cells. After licensing, the dendritic cell, $D(t)$, is free to interact with all T cells, causing them to activate.

The T-cell and dendritic cell populations are subdivided in order to account for the dynamic delays in activation observed in experiments (Mempel et al., 2004). In addition, the subdivision allows the various immunosuppressive effects which occur at different steps in the T-cell activation sequence to be properly included.

The selection of relevant cytokines was motivated by the literature. IL-2, denoted by the variable $C(t)$, is not only a key proliferative cytokine for T cells, but also a current option for immunotherapy (Rosenberg and Lotze, 1986; Dudley et al., 2002). It is necessary to include IL-2 in order to include other suppressive effects, as IL-2 plays a role in balancing the ratio of Tregs to other T cells (Setoguchi et al., 2005). For the suppressive cytokines, TGF-β and IL-10, denoted by $S(t)$ and $I(t)$ respectively, are considered to be important suppressors of T-cell activity, as described above. These molecules are produced by both tumor cells (Gastl et al., 1993; Alleva et al., 1994; Danforth and Sgagias, 1996; Hsieh et al., 2000; Avradopoulos et al., 1997) and Tregs (Liyanage et al., 2002; Jarnicki et al., 2006). All the molecular concentrations in this model are expressed in ng/ml.

The subset of equations describing the response of the immune system to antigen functions realistically in the absence of tumor-induced immunosuppression. This ensures that any tumor-associated suppressive effects are properly scaled with respect to the innate immune response. The tumor–immune interactions and the associated suppression caused by Tregs, TGF-β, and IL-10 are added to this model of T-cell activation.

While other suppressive cytokines and cell types exist, these 12 variables are the important players in the evolution of the tumor–immune system and have been described extensively in the experimental and clinical literature.

Fig. 1 shows a detailed view of the interactions modeled in this paper. The tumor cells produce antigen, which is collected by dendritic cells. These dendritic cells then interact with three T-cell types: effector T cells, helper T cells, and Tregs. The Tregs produce suppressive molecules TGF-β and IL-10 and also directly suppress the activity of the immune system. All three of these T-cell types are expanded due to antigen presentation by the dendritic cells. Tregs also expand through the conversion of helper T cells into Tregs, which adds another feedback mechanism to the model. The fate of the tumor therefore depends on the outcome of the competition between cytotoxic and suppressive effects.
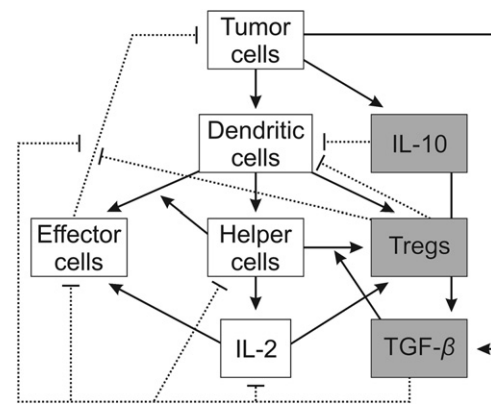

Fig. 1. A diagram showing the interactions that are used in the model. Dotted lines and gray boxes show the suppressive mechanisms.

3.2. Equations

3.2.1. Tumor cells

In the model, the evolution of tumor cells (T) is governed by

$$\dot{T} = \frac{T}{\left(\left(\frac{1}{\gamma_1}\right)^p + \left(\frac{T^{1-m}}{\gamma}\right)^p\right)^{1/p}} - \frac{r_0 T^*}{\left(1+k_2\frac{T^*}{E}\right)} \cdot \frac{1}{\left(1+k_3\frac{R}{E}\right)\left(1+\frac{S}{S_1}\right)}, \quad (1)$$

where γ_1 is given by

$$\gamma_1 = \gamma(T_1)^{m-1} \quad (2)$$

and T^* is given by

$$T^* = \frac{T}{\left(1+\left(\frac{T^{1-n}}{k_1}\right)^p\right)^{1/p}}. \quad (3)$$

The first term on the right hand side of Eq. (1) accounts for tumor growth. Previously, the growth law for a tumor has been modeled in several ways, including logistic (Arciero et al., 2004; de Pillis et al., 2005; Kuznetsov et al., 1994) and Gompertzian (Norton, 1988) models. Experimental data for different types of tumors under different conditions exhibit different growth curves, so there is no universal choice in general. The growth of tumor cells in Eq. (1) is modeled as a mixture between exponential and power law growth.

The doubling time of a tumor scales with tumor size (Skipper, 1971). This indicates that tumors do not follow a purely exponential growth law. The reason for this reduction in effective growth rate is not fully understood. Several mechanisms have been proposed and modeled mathematically, including limitation of nutrient availability (Roose et al., 2007), angiogenesis (Anderson and Chaplain, 1998), and mechanical stress (Byrne and Preziosi, 2003; Ambrosi and Mollica, 2004). Cell signaling may also play a role.

Power law growth has shown to be a good fit for breast cancer, when the tumor is of clinical size (Hart et al., 1998). The general equation for power law growth of a population is

$$\dot{T} = \gamma T^m, \quad (4)$$

where γ is the growth coefficient and m is the power law exponent.

The power growth law breaks down at smaller tumor sizes, since the doubling time approaches zero as the tumor volume goes to zero. For this reason, it is unreasonable to use the power law to model growth for very small tumors, since the maximum doubling time of a tumor is physically limited by cell cycle dynamics. Evidence has shown that large, slow-growing tumors

with lengthy doubling times of several months will exhibit exponential growth with short doubling times on the order of 1–2 days, when the cells are separated from the tumor mass and cultured (Skipper, 1971). Therefore, an exponential growth law is used at small tumor sizes. The equation for exponential growth of a population is given by

$$\dot{T} = \gamma_1 T, \tag{5}$$

where γ_1 is the exponential growth coefficient.

An assumption made in this study is that a tumor with a small power law growth coefficient γ will have a correspondingly small exponential growth coefficient γ_1. The relationship between γ and γ_1 cannot be experimentally determined in vivo, since it is rare to detect very small tumors within the human body, and even rarer to allow them to grow large and subsequently measure their growth properties at different sizes. Therefore, the value of γ_1 is chosen so that the two growth rates match at a transition size $T_1 = 10^6$ cells. This transition size was determined from Steele (1977), with the value of γ_1 calculated by Eq. (2). The transition between these two modes of growth is smooth; the exponent p determines the smoothness of the transition. The parameter γ will be used as one of the two fundamental control parameters in the model, in order to account for tumors that grow at different rates.

The second term of Eq. (1) describes tumor cell kill by effector cells (E), which is the only mechanism for tumor cell death in the model. The first fraction in this term accounts for tumor cell death in the absence of suppressive effects. The parameter r_0 is the rate at which an effector cell kills a tumor cell. The total rate of tumor cell killing depends on the ratio of tumor cells and effector cells. When this ratio is high (effector cell numbers are small compared to tumor cell numbers), each effector cell has access to many tumor cells, and thus the killing rate is on the order of $r_0 E/k_2$, proportional to the number of effector cells. When effector cell counts are much larger than tumor cell counts, the killing rate saturates to a level dependent on tumor cells only ($r_0 T^*$), since additional effector cells entering the system will not contribute significantly to the tumor cell killing rate, due to crowding effects. The parameter k_2 controls the shape of the interaction curve when cell counts are comparable in number. Since the simulation is not intended for small values of E or T approaching zero, the singularity potentially caused by the term T/E is of no concern.

The variable T^* represents the number of tumor cells which are accessible by the immune system. Poor vascularization of a growing tumor limits the access of immune cells to the entire tumor (Jain and Ward-Hartley, 1984; Tannock et al., 2002). For small tumor sizes, the entire tumor is accessible to the immune cells. As the tumor grows larger, only an outer shell of the tumor is sufficiently perfused with blood vessels to allow immune cell access (Jain and Ward-Hartley, 1984). This transition occurs at approximately the same size as the transition in the growth law, since both have a dependence on blood vessel perfusion depths. In the model, T^* is used in place of T whenever the interactions are dependent on the spatial access to the tumor cells. For example, production of TGF-β can be expected in all functional tumor cells, and therefore T is used for that process. The interaction of CD8$^+$ effector T cells and tumor cells, however, requires physical contact, and therefore effector cells primarily encounter the perfused tumor mass, T^*.

The second fraction in the second term of Eq. (1) represents the suppressive effects of Tregs and TGF-β on the cytotoxicity. The term $1 + k_3(R/E)$ represents the effect of Tregs (R) on the effector cells' killing rate (Piccirillo and Shevach, 2001). The suppression is ratio dependent, with parameter k_3 controlling the shape of the interaction, so that increased Treg to effector T cell ratios will decrease the tumor cell killing rate. The term $1 + (S/S_1)$ represents

suppression of effector cell activity due to TGF-β (S), which has been shown to reduce the cytotoxicity of effector T cells (Thomas and Massagué, 2005). The parameter S_1 is the TGF-β concentration where killing is suppressed by half.

There is no explicit term for natural death of tumor cells; rather, it is taken into account in the growth term. Although there is evidence that TGF-β can promote tumor growth (Fitzpatrick et al., 1996), this effect is not included in this study.

3.2.2. Dendritic cells

Mature dendritic cells evolve according to

$$\dot{U} = \frac{aT^*}{\left(1 + \frac{I}{I_1}\right)\left(1 + \frac{R}{R_1}\right)} - \frac{\lambda U}{1 + \frac{U}{M_H}} - \delta_U U \tag{6}$$

and

$$\dot{D} = \frac{\lambda U}{1 + \frac{U}{M_H}} - \delta_D D, \tag{7}$$

where U represents the number of unlicensed dendritic cells, and D is the number of licensed dendritic cells. The first term of Eq. (6) describes the maturation of dendritic cells by an encounter with tumor antigen. The antigenicity of a tumor, denoted by the parameter a, is known to vary widely among different types of tumors (Chen et al., 1994; Kripke, 1974), and is taken as the second control parameter in this study.

The maturation process is inhibited by Tregs and IL-10 (Larmonier et al., 2007), represented by the two suppressive denominator terms. Following the previous discussion of effector cells, the difficulty of accessing the tumor interior by immune cells is reflected by the use of T^*. The model assumes that there is a constant pool of immature dendritic cells which circulate in the body searching for antigens. This constant is effectively included in the parameter a.

The second term of Eq. (6) and the first term of Eq. (7) account for the licensing of dendritic cells upon encounter with helper T cells. This licensing process depends on the ratio of the two cell types. For small numbers of dendritic cells, licensing helper T cells are abundant, and the process goes as λU. For high numbers of dendritic cells, the rate is limited by the availability of helper cells, so the licensing is on the order of λM_H. Eqs. (6) and (7) both include terms to account for cell death or deactivation after a characteristic time period, given by δ_U and δ_D.

3.2.3. Memory T cells

All three types of T cells in the model are activated in the same basic way. The memory cells enter a brief activation phase where proliferation is rapid, and then they become fully functional T cells. The total memory population M is defined by

$$M \equiv M_E + M_H + M_R, \tag{8}$$

where the right hand terms are the constant populations of effector memory T cells, helper memory T cells, and Treg memory cells, respectively.

3.2.4. CD8$^+$ effector T cells

CD8$^+$ effector T cells follow

$$\dot{A_E} = \frac{\alpha_1 M_E}{1 + k_4 \frac{M}{D}} - \delta_A A_E \tag{9}$$

and

$$\dot{E} = \frac{\alpha_2 A_E C}{\left(1 + \frac{S}{S_2}\right)(C_1 + C)} - \delta_E E. \tag{10}$$

The first term of Eq. (9) activates the effector memory cells, in the presence of mature licensed dendritic cells. Again, this process is

ratio-dependent. As dendritic cell numbers increase, the term saturates to $\alpha_1 M_E$. The second term describes the expiration of the activated phase of these cells.

The first term of Eq. (10) gives the proliferation of CD8$^+$ effector cells. This depends on the presence of activated cells and the proliferative cytokine IL-2 (C). As IL-2 increases, the level of proliferation reaches a maximum of $\alpha_2 A_E$ in the absence of suppression. TGF-β (S) suppresses T-cell proliferation (Thomas and Massagué, 2005; McKarns and Schwartz, 2005); the parameter S_2 is included to account for this effect. The second term accounts for effector cell death or inactivation, with parameter δ_E.

3.2.5. CD4$^+$ helper T cells

Helper T cells follow a similar activation path as effector T cells

$$\dot{A_H} = \frac{\alpha_3 M_H}{1+k_4 \frac{M}{(U+D)}} - \delta_A A_H \tag{11}$$

and

$$\dot{H} = \frac{\alpha_4 A_H C}{\left(1+\frac{S}{S_2}\right)(C_1+C)} - \frac{\alpha_7 H S}{S_3+S} - \delta_H H. \tag{12}$$

These two equations differ from those for the effector T cells in two ways. First, the activation of memory helper cells can be prompted by both licensed and unlicensed dendritic cells (Smith et al., 2004). Second, helper T cells can be converted into Tregs in the presence of TGF-β (Liu et al., 2007b), and this is represented by the second term in Eq. (12). As TGF-β increases, the rate of change from helper cells to Tregs saturates at $\alpha_7 H$.

3.2.6. CD4$^+$ CD25$^+$ Foxp3$^+$ regulatory T cells

Tregs follow a similar pair of equations

$$\dot{A_R} = \frac{\alpha_5 M_R}{1+k_4 \frac{M}{D}} - \delta_A A_R \tag{13}$$

and

$$\dot{R} = \frac{\alpha_6 A_R C}{(C_1+C)} + \frac{\alpha_7 H S}{S_3+S} - \delta_R R. \tag{14}$$

The principal difference here is that Treg proliferation is not suppressed by TGF-β, in contrast to the other T-cell populations.

3.2.7. Cytokines and molecules

The proliferative cytokine IL-2 is produced by activated helper cells, and the concentration is given by

$$\dot{C} = \frac{p_C A_H}{\left(1+\frac{S}{S_4}\right)\left(1+\frac{I}{I_2}\right)} - \frac{C}{\tau_C}. \tag{15}$$

The first term of Eq. (15) represents the production of IL-2 by the activated helper cells. This production is inhibited by TGF-β (Thomas and Massagué, 2005; McKarns and Schwartz, 2005) and IL-10 (Taga et al., 1993; de Waal Malefyt et al., 1993). The second term represents the removal of IL-2 from the system, with characteristic time τ_C.

TGF-β and IL-10 are produced by both tumor cells and Tregs, and follow

$$\dot{S} = p_1 R + p_2 T - \frac{S}{\tau_S} \tag{16}$$

and

$$\dot{I} = p_3 R + p_4 T - \frac{I}{\tau_I}. \tag{17}$$

The first terms of each equation represent the production by Tregs, the second terms represent production by tumor cells,

and the final terms represent the removal from the system with characteristic times τ_S and τ_I.

For convenience, all 12 equations are collected here.

$$\dot{T} = \frac{T}{\left(\left(\frac{1}{\gamma_1}\right)^p + \left(\frac{T^{1-m}}{\gamma}\right)^p\right)^{1/p}} - \frac{r_0 T^*}{\left(1+k_2 \frac{T^*}{E}\right)} \cdot \frac{1}{\left(1+k_3 \frac{R}{E}\right)\left(1+\frac{S}{S_1}\right)}, \tag{18}$$

$$\dot{U} = \frac{aT^*}{\left(1+\frac{I}{I_1}\right)\left(1+\frac{R}{R_1}\right)} - \frac{\lambda U}{1+\frac{U}{M_H}} - \delta_U U, \tag{19}$$

$$\dot{D} = \frac{\lambda U}{1+\frac{U}{M_H}} - \delta_D D, \tag{20}$$

$$\dot{A_E} = \frac{\alpha_1 M_E}{1+k_4 \frac{M}{D}} - \delta_A A_E, \tag{21}$$

$$\dot{E} = \frac{\alpha_2 A_E C}{\left(1+\frac{S}{S_2}\right)(C_1+C)} - \delta_E E, \tag{22}$$

$$\dot{A_H} = \frac{\alpha_3 M_H}{1+k_4 \frac{M}{(U+D)}} - \delta_A A_H, \tag{23}$$

$$\dot{H} = \frac{\alpha_4 A_H C}{\left(1+\frac{S}{S_2}\right)(C_1+C)} - \frac{\alpha_7 H S}{S_3+S} - \delta_H H, \tag{24}$$

$$\dot{A_R} = \frac{\alpha_5 M_R}{1+k_4 \frac{M}{D}} - \delta_A A_R, \tag{25}$$

$$\dot{R} = \frac{\alpha_6 A_R C}{(C_1+C)} + \frac{\alpha_7 H S}{S_3+S} - \delta_R R, \tag{26}$$

$$\dot{C} = \frac{p_C A_H}{\left(1+\frac{S}{S_4}\right)\left(1+\frac{I}{I_2}\right)} - \frac{C}{\tau_C}, \tag{27}$$

$$\dot{S} = p_1 R + p_2 T - \frac{S}{\tau_S}, \tag{28}$$

$$\dot{I} = p_3 R + p_4 T - \frac{I}{\tau_I}, \tag{29}$$

where

$$\gamma_1 = \gamma(T_1)^{m-1} \tag{30}$$

and

$$T^* = \frac{T}{\left(1+\left(\frac{T^{1-n}}{k_1}\right)^p\right)^{1/p}}. \tag{31}$$

This is a system of 12 ODEs with 41 parameters. The model has two control parameters γ and a representing, respectively, growth rate and antigenicity of the tumor. The remaining 39 parameters are given in Tables 1–4, following the analysis given in the next section.

4. Parameter estimation

The model of tumor–immune interactions given in Eqs. (18)–(31) was constructed so that the parameters could be derived from the literature. Although *in vivo* data for one type of cancer growing in one species would be the optimal method of acquiring the necessary parameters, such a comprehensive data set does not exist. Therefore, parameters come from a diverse set of experiments. Whenever possible, experiments using human *in vivo* measurements were used, but a number of parameters are only feasibly measured *in vitro* or in murine models. It is noted that parameters measured *in vitro* are sometimes different than the values *in vivo*, and therefore this is a

Table 1
Parameter values for tumor progression, Eqs. (18), (30), and (31).

Parameter	Value	Units	References
γ	100–1000	$\text{cell}^{1-m}\,\text{day}^{-1}$	Friberg and Mattson (1997)
			Iwashita et al. (1998)
			Jackson et al. (1984)
			Peer et al. (1993)
γ_1	0.1–1	day^{-1}	
T_1	10^6	cell	Steele (1977)
m	$\frac{1}{2}$		Hart et al. (1998)
n	$\frac{2}{3}$		Jain and Ward-Hartley (1984)
p	3		
r_0	0.9	day^{-1}	Diefenbach et al. (2001)
			Dudley et al. (2002)
			Thomas and Massagué (2005)
k_1	100	cell^{1-n}	Jain and Ward-Hartley (1984)
			Steele (1977)
k_2	1.2		Dudley et al. (2002)
k_3	11		Piccirillo and Shevach (2001)
S_1	3.5	ng ml^{-1}	Thomas and Massagué (2005)

Table 2
Parameter values for dendritic cell expansion, Eqs. (19) and (20).

Parameter	Value	Units	References
a	10^{-5}–10^5	day^{-1}	
λ	0.5	day^{-1}	Smith et al. (2004)
δ_U	0.14	day^{-1}	Liu et al. (2007a)
δ_D	0.5	day^{-1}	Liu et al. (2007a)
I_1	0.4	ng ml^{-1}	Larmonier et al. (2007)
R_1	2×10^7	cell	Larmonier et al. (2007)

Table 3
Parameter values for T-cell expansion, Eqs. (21)–(26).

Parameter	Value	Units	References
α_1	23	day^{-1}	Mempel et al. (2004)
α_2	16	day^{-1}	Mempel et al. (2004)
α_3	9.9	day^{-1}	Mempel et al. (2004)
α_4	1.9	day^{-1}	Mempel et al. (2004)
α_5	5.1	day^{-1}	Mempel et al. (2004)
α_6	2.1	day^{-1}	Mempel et al. (2004)
α_7	0.022	day^{-1}	Woo et al. (2001)
			Liyanage et al. (2002)
			Wolf et al. (2003)
			Liu et al. (2007b)
M	10^7	cell	Arstila et al. (1999)
			Harty and Badovinac (2008)
k_4	0.33		Mempel et al. (2004)
C_1	0.3	ng ml^{-1}	Thomas and Massagué (2005)
S_2	2.9	ng ml^{-1}	Thomas and Massagué (2005)
			McKarns and Schwartz (2005)
S_3	1.7	ng ml^{-1}	Liu et al. (2007b)
δ_A	0.2	day^{-1}	Mempel et al. (2004)
δ_E	1.0	day^{-1}	Yates and Callard (2001)
δ_H	0.1	day^{-1}	Yates and Callard (2001)
δ_R	0.1	day^{-1}	Yates and Callard (2001)
			Vukmanovic-Stejic et al. (2006)

Table 4
Parameter values for IL-2, TGF-β and IL-10 concentrations, Eqs. (27)–(29).

Parameter	Value	Units	References
p_C	1.7×10^{-5}	$\text{ng ml}^{-1}\,\text{cell}^{-1}\,\text{day}^{-1}$	McKarns and Schwartz (2005)
p_1	1.8×10^{-8}	$\text{ng ml}^{-1}\,\text{day}^{-1}\,\text{cell}^{-1}$	Liyanage et al. (2002)
p_2	1.1×10^{-7}	$\text{ng ml}^{-1}\,\text{day}^{-1}\,\text{cell}^{-1}$	Danforth and Sgagias (1996)
p_3	1.4×10^{-8}	$\text{ng ml}^{-1}\,\text{day}^{-1}\,\text{cell}^{-1}$	Liyanage et al. (2002)
p_4	1.3×10^{-10}	$\text{ng ml}^{-1}\,\text{day}^{-1}\,\text{cell}^{-1}$	Gastl et al. (1993)
I_2	0.75	ng ml^{-1}	Taga et al. (1993)
			de Waal Malefyt et al. (1993)
S_4	0.9	ng ml^{-1}	Thomas and Massagué (2005)
			McKarns and Schwartz (2005)
τ_C	0.08	day	Skog et al. (2001)
			Konrad et al. (1990)
			Lotze et al. (1985)
τ_S	0.07	day	Wakefield et al. (1990)
τ_I	0.05	day	Le et al. (1997)

4.1.1. Determination of tumor growth parameters

In this study, the growth law for large tumors is chosen to be a power law, based on experimental evidence (Hart et al., 1998). Small tumors follow exponential growth. The transition is matched at a transition size of $T_1 = 10^6$ cells, and is smoothed by the exponent p, estimated from growth curves presented in Steele (1977). Variation of p does not significantly affect the results of the model. The value of p determines the size of the transition zone from exponential to power law growth. The choice of $p = 3$ corresponds to a transition zone of about 2 orders of magnitude in tumor size. This means that below a size of 10^5 cells, the tumor is growing exponentially, above 10^7 cells, the tumor is following the power law, and between 10^5 and 10^7 cells, the tumor transitions smoothly between these two growth laws.

The value of $m = 0.5$ is taken directly from Hart et al. (1998). With the choice of m, the growth coefficient γ can be calculated for a given tumor by measuring the doubling time t_d and initial detection size T_d. The growth coefficient is given by

$$\gamma = \frac{T_d^{1-m}}{t_d(1-m)}(2^{1-m}-1). \tag{32}$$

Assuming a detection size of $T_d = 10^9$ cells, a growth exponent $m = 0.5$, and using the range of doubling times given in Friberg and Mattson (1997), Iwashita et al. (1998), Jackson et al. (1984), and Peer et al. (1993) for various cancer types, the biological range of the growth coefficient is approximately $100 < \gamma < 1000$, where the units of γ are given in Table 1.

For the range of values for γ determined above, this gives a corresponding range for γ_1 between 0.1 and 1, using Eq. (30). Equivalently, this gives a range of cellular doubling times between 0.7 and 7 days, which is a biologically reasonable range for cell cycle durations.

4.1.2. Determination of effective tumor size parameters

The parameters n and k_1 determine the effective tumor size, with respect to the immune system accessibility. Experimental evidence shows that growing tumors exhibit a perfusion depth of approximately 500 μm (Jain and Ward-Hartley, 1984), suggesting that a tumor of up to 1 mm in size is fully accessible to the immune system. Once the tumor crosses this threshold, only an outer shell of tumor cells will be accessible. The effective tumor size is therefore equal to T when the tumor is small, and proportional to the surface area ($T^{2/3}$) when the tumor is large. The parameter n is 2/3, and the parameter k_1 is chosen so that the transition between these two regimes occurs at 1 mm in size, or

source of error in the model. However, as more *in vivo* measurements become available in the future, the model can be updated to reflect this new information.

4.1. Parameter values for tumor progression

Table 1 shows the parameter values for Eqs. (18), (30), and (31).

10^6 cells. As with the tumor growth law, the exponent p is used to smooth the transition from T to T^*.

4.1.3. Determination of tumor cytotoxicity parameters

The parameters r_0 and k_2 were taken from *in vitro* T-cell lysis data presented in Diefenbach et al. (2001), Dudley et al. (2002), and Thomas and Massagué (2005). The level of tumor cell lysis at high T-cell to tumor cell ratios was used to estimate a value for r_0. Since 20–60 percent of tumor cells are killed after 4 h, the range of killing rates is approximately 1.5–8 cells per day. However, the value used in the study was chosen more conservatively, since the effector cells have to migrate to the tumor site, diffuse into the tumor, and lyse the cells. In the absence of a compartmentalized model, this parameter has to incorporate these effects. Transit time for effector T cells to move from the lymph node to the tumor site can take many hours (von Andrian and Mackay, 2000), and it is likely that a sizeable fraction of the cells do not find the tumor. Once the cells arrive at the tumor, they must diffuse through the tumor, a process which also may last for several hours (Boissonnas et al., 2007). Finally, the cytotoxic interactions between the CTL and the tumor can last from 2 to 8 h (Waterhouse et al., 2006; Breart et al., 2008). From the data cited above, r_0 was estimated to be approximately 0.9. Parameter k_2 was chosen so that the shape of the lysis curve was approximated at different E/T ratios.

4.1.4. Determination of immunosuppressive parameters

The value of k_3 was estimated so that the dependence of suppression on the R/E ratio matched the data given in Piccirillo and Shevach (2001). The suppression of tumor cell killing by TGF-β was calculated from the data (Thomas and Massagué, 2005) that measured the effectiveness of tumor lysis in the presence and absence of 100 pM (4.5 ng/ml) TGF-β. The parameter S_1 represents the concentration at which lytic capability is cut by half. Since 4.5 ng/ml suppressed the cytotoxicity by a little more than half, the value of 3.5 ng/ml was chosen for S_1.

4.2. Parameter values for dendritic cell expansion

Table 2 shows the parameter values used in Eqs. (19) and (20).

4.2.1. Determination of dendritic cell maturation and licensing parameters

The value of the parameter a, which represents the antigenicity of a tumor, exhibits significant variation between different tumor types (Kripke, 1974). To account for the large intertumor heterogeneity in both growth rate and antigenicity, ranges of values are used for these parameters. Unlike the growth parameter, where cell cycle times and tumor growth measurements can guide the selection of an appropriate range, the antigenicity is more difficult to determine. In this work, the upper limit for antigenicity was chosen based on dendritic cell numbers. There is no inherent limitation in the model that prevents unlimited dendritic cell expansion; therefore, the upper limit of 10^5 for antigenicity is chosen because dendritic cell counts in the model are maintained at biologically reasonable levels for antigenicities up to this value. There is no expected lower limit for antigenicity, since theoretically a tumor may not elicit any immune response at all. Below a value of $a = 10^{-5}$, however, the immune response is so low that further reduction of the antigenicity parameter does not offer qualitatively different results.

Data from Smith et al. (2004) provided the parameter λ. Dendritic cells licensed by T cells begin to appear after 24 h, so we estimate licensing rate to be approximately 0.5 per day. The death rate of mature dendritic cells, δ_U, was taken from

experiments measuring the turnover of dendritic cells that had been primed with antigen (Liu et al., 2007a). The parameter δ_D, which represents the expiration of antigen presentation of the licensed dendritic cells, was calculated using dendritic cell dynamics measured in Mempel et al. (2004), described in Section 4.3.1.

4.2.2. Determination of dendritic cell immunosuppression parameters

The suppression of dendritic cell maturation by IL-10 and Treg cells was calculated from experiments in Larmonier et al. (2007). Expression of the maturation marker Interleukin-12 (IL-12) was measured in dendritic cell cultures. IL-10, TGF-β and Tregs all partially abrogated the maturation process. The data for TGF-β were not sufficient to establish a suppressive term in Eq. (19), but parameters I_1 and R_1 for IL-10 and Tregs were calculated based on the concentrations at which the maturation markers were expressed at half-normal levels.

4.3. Parameter values for T-cell expansion

Table 3 shows the parameter values used in Eqs. (21)–(26).

4.3.1. Determination of T-cell activation and proliferation parameters

The parameter k_4 relates to the number of T cells that can interact with a dendritic cell at any given time. This value can vary between 3 and 8, and here it is assumed to be approximately 5 (Romani et al., 1989; De Boer and Perelson, 1994); k_4 therefore controls the shape of the activation curve of T cells as the ratio of dendritic cells to T cells varies.

With the selection of k_4, the parameters relating to CD8$^+$ T-cell activation and proliferation were calculated by separating the equations relating to these populations and finding parameters which resulted in the dynamics outlined by Mempel et al. (2004), assuming that T cells expand about 3–4 orders of magnitude upon encounter with antigen (Harty and Badovinac, 2008). Briefly, 5×10^5 dendritic cells (D) and zero effector T cells (A_E and E) were used as initial conditions in the simplified model shown in Eqs. (33)–(35).

$$\dot{D} = -\delta_D D, \tag{33}$$

$$\dot{A}_E = \frac{\alpha_1 M}{1 + k_4 \frac{M}{D}} - \delta_A A_E, \tag{34}$$

$$\dot{E} = \alpha_2 A_E - \delta_E E. \tag{35}$$

These three equations are equivalent to Eqs. (20)–(22) from the full model, modified so that there is no source of dendritic cells, ample concentration of IL-2, and no TGF-β. The value of M was set to 10^4 cells. This simulation was used to determine parameters $\delta_D, \alpha_1, \delta_A, \alpha_2$ and δ_E. The activation stage lasts between 20 and 24 h (Mempel et al., 2004), followed by proliferation into full effector cells.

The value of M used in the simulations was 10^7 cells. The number of different antigen-specific T cells in the human body has been estimated to be approximately 10^6–10^7 clones (Arstila et al., 1999). Given a total T-cell population of 10^{11} cells, this suggests that there are approximately 10^4–10^5 T cells that are specific to each antigen. After encountering an antigen, naive cells expand into memory cells, and this expansion can be as large as four orders of magnitude (Harty and Badovinac, 2008). Therefore, the memory cell population specific to an antigen is on the order of 10^7–10^9 cells. We have chosen constant M to be on the lower end of this range, to be conservative. The value of this constant does not have a significant effect on the long-term behavior of the

tumor growth. Order-of-magnitude changes only had a minimal quantitative effect. Simulations performed with a time-varying M, by starting M at 10^4 cells and increasing to 10^7 over the course of a few weeks to simulate naive to memory transition, also showed little effect.

The typical ratio of $CD4^+$ to $CD8^+$ T cells in a healthy individual is approximately 2:1 (Taylor et al., 1989). This is reflected in the 2:1 split of these cells in the breakdown of the constant M into $M_H = 0.6\,M$ and $M_E = 0.3\,M$. The remaining part of the memory cell constant is occupied by $M_R = 0.1\,M$. In a typical expansion, $CD4^+$ T cells will expand about one-fourth as much as $CD8^+$ T cells (Haring et al., 2001). The parameters α_3, α_4, and δ_H were selected so that the final ratios were approximated during expansion.

Tregs occupy between 3 and 10 percent of the T-cell compartment during normal immune reactions (Seddiki et al., 2006). In a normal immune response, Tregs are assumed to expand with similar rates as helper cells, while maintaining the same ratio. The parameters α_5, α_6 and δ_R were selected so that Treg expansion followed these constraints. In cancer patients, it is known that Treg percentages are increased to as much as 20–30 percent (Woo et al., 2001; Liyanage et al., 2002; Wolf et al., 2003). This effect is accounted for by conversion of helper T cells into Tregs, as described in Section 4.3.2.

The parameters C_1 and S_2, which control the saturation of T-cell proliferation by IL-2 and TGF-β respectively, were calculated from experiments in Thomas and Massagué (2005) and McKarns and Schwartz (2005). The concentrations which produced half-maximal proliferation were estimated from the data showing T-cell proliferation for different concentrations of IL-2, and also in the presence or absence of TGF-β.

4.3.2. Parameters for conversion of helper T cells into Tregs

The parameters for the conversion of helper T cells into Tregs are based on systemic levels of TGF-β (Wakefield et al., 1990; Desser et al., 2001; Liu et al., 2007b) and Treg to T-cell ratios in cancer patients (Woo et al., 2001; Liyanage et al., 2002; Wolf et al., 2003). With the tumor established in the model, the parameter α_7 was chosen so that Treg levels were in agreement with R/E ratios seen in vivo, for a given tumor size.

4.4. Parameter values for IL-2, TGF-β and IL-10 concentrations

Table 4 shows the parameter values for Eqs. (27)–(29).

4.4.1. Determination of molecular production rates

Production of IL-2 by helper T cells was determined from in vitro experiments given in McKarns and Schwartz (2005). Briefly, helper T cells were cultured at a concentration of 10^5 cells/ml, with the appropriate activation factors. The concentration of IL-2 after 24 h was found to be 1 ng/ml. Assuming that the production did not saturate in 24 h, the production rate of IL-2 was 10^{-5} ng/cell per day. The production of IL-2 is relevant in the lymph nodes where T-cell activation occurs. Given a typical lymph node size of 0.6 ml (Kim et al., 2002), the production rate with respect to concentration is 1.7×10^{-5} ng/ml per cell per day.

Production rates for IL-10 and TGF-β by Tregs and tumor cells were calculated in similar fashion, from in vitro data given in Liyanage et al. (2002), Danforth and Sgagias (1996), and Gastl et al. (1993). In the absence of a spatially-resolved compartmental model, it should be noted that these production parameters will necessarily be rough average estimates, since the concentration of these cytokines will vary spatially due to heterogeneous production rates, diffusion, and autocrine and paracrine effects.

4.4.2. Determination of molecular clearance rates

The clearance time of IL-2, τ_C, was estimated from human in vivo data given in Skog et al. (2001), Konrad et al. (1990), and Lotze et al. (1985). The values for the half life of IL-2 in the human body ranged from 0.02 to 0.17 days. A representative value of 0.08 days was chosen. The same method was used to estimate clearance times for TGF-β and IL-10 using the references shown in Table 4.

4.4.3. Determination of S_4 and I_2

Suppression of IL-2 production by TGF-β was calculated from experiments in Thomas and Massagué (2005) and McKarns and Schwartz (2005). IL-2 production for a given concentration of TGF-β was used to calculate the concentration of TGF-β which cut the IL-2 production in half.

IL-10 suppression of IL-2 production is given in Taga et al. (1993) and de Waal Malefyt et al. (1993) for two different concentrations of IL-10. These data were fit and the concentration of IL-10 that caused the IL-2 production to be halved was estimated to be 0.75 ng/ml.

5. Results and discussion

5.1. Main qualitative behaviors

The system of ODEs was solved numerically using MATLAB (published by Mathworks, Natick, MA). For a given set of immune system parameters, the effectiveness of the immune system against the tumor depends on the two control parameters, tumor antigenicity and tumor growth rate. Fig. 2 shows the results of the model for various values of the growth rate and antigenicity. The horizontal axis represents increasing tumor antigenicity, and the vertical axis represents increasing tumor growth rate. The axis
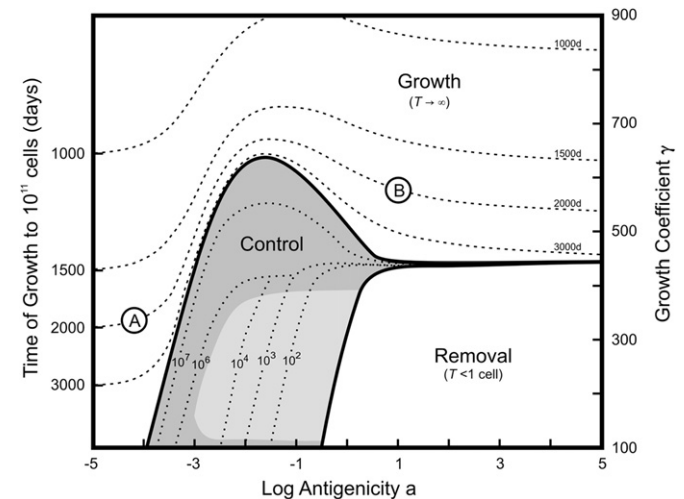

Fig. 2. The long-term behavior of a tumor. Control parameters are the antigenicity a, on the horizontal axis, and tumor growth rate γ, on the right-hand vertical axis. The left-hand vertical axis shows the time it takes the tumor to reach 10^{11} cells in the absence of any immune system killing. The area marked *Growth* consists of tumors that grow without bound, *Removal* denotes complete cure of the tumor by the immune system (i.e., T goes below one cell), and *Control* denotes maintenance of the tumor at either a stable fixed point or a stable limit cycle. The dashed lines in the *Growth* area show the time it takes for the tumor to reach 10^{11} cells. The dotted lines in the *Control* area show the values of the fixed points. The lighter gray area in the *Control* section denotes tumors which display a stable limit cycle, and contours passing through this region give the value of the central unstable fixed point. The darker gray area accounts for tumors which grow to stable fixed points. Circled letters refer to simulations shown in Figs. 6 and 7.

labels on the left show the time it would take a tumor to reach 10^{11} cells (representing a lethal volume) in the absence of any immune system response (i.e., setting parameter $r_0 = 0$). The axis labels on the right show the corresponding values of the control parameter γ. Long-term behavior of the tumor was determined for the ranges of the two control parameters shown on the axes, using fixed point analysis (described in Section 5.3). The long-term behavior of the tumor has three possible outcomes: tumor removal, considered to occur when the value of T falls below 1 cell; tumor control, which occurs if the tumor is bounded, reaching either a stable fixed point or a stable limit cycle; or unbounded growth. The initial conditions for all simulations were $T_0 = 1$ cell; other cell populations were set to zero, except for E and D, which were set to a small value (10^{-5}) to avoid singularities. Since the values of D and E rapidly increase, there is no potential for division-by-zero errors in the simulations. Initial conditions for the cytokines were set to zero.

The area marked *Control* represents the tumors that either reach a steady state greater than one cell or oscillate around a size greater than one cell. The immune system killing rate and the tumor growth rate in Eq. (18) reach an equilibrium. The dotted contour lines in Fig. 2 within the *Control* section show the equilibrium size of the tumor for a given combination of growth rate and antigenicity. For some parameter values, represented by the darker gray area, the tumor reaches a stable fixed point. The lighter gray area shows tumors that oscillate within a stable limit cycle (see Section 5.3).

The stable size of the tumor is always between 1 cell and about 10^8 cells. Fixed points with tumor sizes greater than 10^8 cells were not observed for any growth rate or antigenicity. This region of stability at a small volume can be viewed as a mechanism by which a tumor can remain dormant for a period. However, it is important to note that the model is deterministic, so that a steady state in the model will persist forever. In the biological situation, conditions are constantly changing, due to tumor cell mutations, health of the host, and other factors. These random effects can destabilize an equilibrium and cause the tumor to begin to grow or be removed.

The area marked *Removal* in Fig. 2 represents the tumors that are removed by the immune system. These tumors are slower-growing and more antigenic, and the immune system is able to kill the tumor cells faster than the tumor is able to grow. Suppression is limited, since Tregs, TGF-β levels, and IL-10 levels never become significant, and the size of the tumor is never large enough to prevent immune cell access to the interior. This region is a subset of the control region: if tumor cells were permitted to exist at a value of a fraction of one cell, they would eventually reach a stable point as well. It is important to note that the boundary of the region of removal is therefore the contour of equilibrium for 1 cell. Given that stochastic effects begin to dominate the dynamics of cell interactions when tumor cell numbers become low, the border of this region is illustrative, rather than being a precise boundary for tumor eradication.

The area marked *Growth* in Fig. 2 shows the tumors which grow without bound, eventually reaching a detectable size (10^9 cells and greater). The dashed lines in the growth section represent contours of the time needed for the tumor to reach 10^{11} cells in size. On the left side of the figure, for $\log a = -5$, the contour lines essentially reach the values determined by free tumor growth shown on the left-hand axis, indicating that for antigenicities less than this value, the immune system has no significant effect on tumor growth. As antigenicity is increased, the immune system does slow down tumor growth within the *Growth* region, up to the optimal value of about $\log a = -1.5$. Further increases in the antigenicity beyond this level will cause the tumor to grow faster than at the optimal antigenicity.

Tumors with high growth rates escape because they grow faster than the immune system can kill them. Of interest is the region of growth to the right of the control peak (point **B**). Even though the antigenicity is higher at point **B** than within the peak of the *Control* region, the tumor grows without bound. In a linear system, increasing the antigenicity would result in an increased response of the immune system, and therefore a more favorable tumor outcome. However, these highly antigenic tumors in the region near point **B** escape because they promote a large increase in Treg populations and TGF-β levels and thus suppress the immune system, despite the high antigenicity. This non-linear and non-monotonic relationship between antigenicity and immune system effect could have important applications in immunotherapies which modulate the effective antigenicity of the tumor. Section 5.5 shows the application of dendritic cell therapy.

5.2. Immunosuppressive effects of TGF-β, converted Tregs, and IL-10

Fig. 3 shows the long-term behavior of the tumor when TGF-β is removed from the system, by setting the value of S to zero. This has two effects on the system: the direct suppressive effects of TGF-β are removed, and the conversion of helper cells to Tregs is stopped. These are the two mechanisms responsible for the existence of the optimal antigenicity peak evident in Fig. 2. When these mechanisms are removed, the fixed point contours continuously increase towards an asymptotic value, rather than displaying a peak. As expected, the *Control* region expands significantly, since much of the immunosuppression has been removed. However, the lower portion of the figure, corresponding to slower growing tumors, is minimally impacted by the change. Tumors which are removed and those which are maintained at a small volume of $T < 10^6$ cells exhibit very similar dynamics as in Fig. 2. This is expected, because conversion of helper cells to Tregs depends on TGF-β, and the level of TGF-β at small tumor sizes is negligible.

Fig. 4 shows the long-term tumor behavior when only the conversion of helper cells to Tregs by TGF-β has been disabled by setting the parameter α_7 to zero. The direct suppressive effects of TGF-β remain in effect. The upper *Control* region has expanded in this figure as well. The peak associated with an optimal antigenicity persists, though shifted to the right about one order of magnitude in antigenicity.
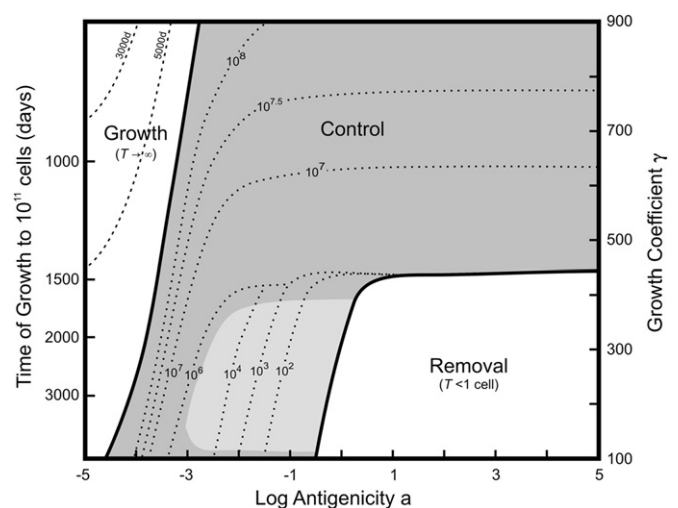

Fig. 3. Tumor responses to the immune system, without conversion of helper cells to Tregs (parameter $\alpha_7 = 0$), and without TGF-β suppression. In contrast with Fig. 2, an optimal antigenicity no longer exists. See caption of Fig. 2 for explanation of regions.
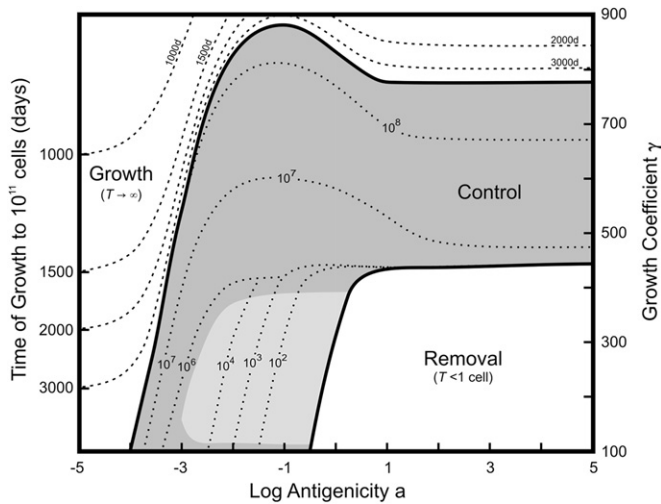
Fig. 4. Tumor responses to the immune system, without conversion of helper cells to Tregs (parameter $\alpha_7 = 0$). See caption of Fig. 2 for explanation of regions.
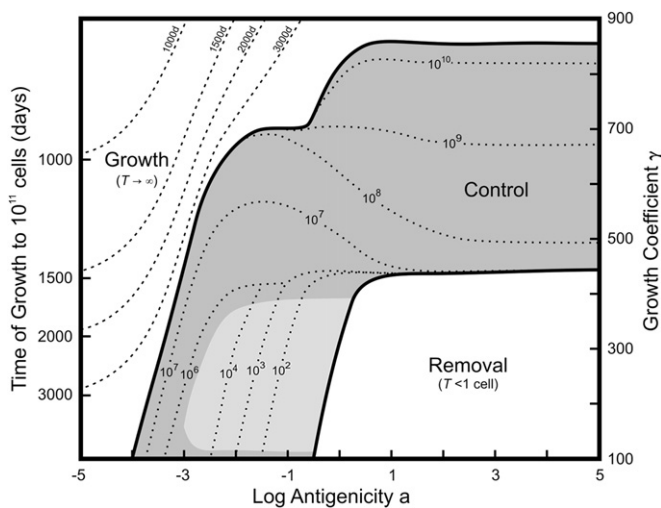

Fig. 5. Tumor responses to the immune system, without the direct effects of TGF-β suppression. Conversion of helper T cells to Tregs remains active. See caption of Fig. 2 for explanation of regions.

The effect of TGF-β suppression on the system is shown in Fig. 5, where the direct suppressive effects of TGF-β have been disabled by removing the suppressive terms associated with parameters S_1, S_2, and S_4 in Eqs. (18), (22), (24), and (27). Conversion of helper T cells into Tregs is still active for this figure. The upper *Control* area is expanded in this case. The existence of an optimal antigenicity persists for tumors that reach a stable size between 10^6 and 10^9 cells. Larger stable tumors can be reached when the antigenicity is high, in contrast to Figs. 2 and 3 where these tumors would grow without bound. These high-stability points do not exhibit an optimal antigenicity profile. As with Fig. 4, the lower portion of the figure for small tumor sizes and removed tumors remains unchanged, due to minimal TGF-β suppression at these levels.

For the production rates of IL-10 found in the literature, IL-10 has a minimal suppressive effect in the model. The production rates of IL-10 would need to be increased by over two orders of magnitude to see a difference in suppression comparable to that seen with Tregs and TGF-β. This is not consistent with experimental evidence showing that for some types of cancer, IL-10 has a significant effect on immunosuppression (Avradopoulos et al., 1997). The

secretion of IL-10 in these cancers may be higher than estimated in this study. It is also possible that IL-10 acts locally in a paracrine fashion, rather than systemically, in which case the magnitude of suppression would be underestimated in the model. This question could be further investigated in a spatially-distributed model.

The importance of various suppressive effects at different stages of tumor growth can be quantified. The overall killing rate of tumor cells by effector T cells is given by the second term of Eq. (18). The unsuppressed rate, r_0 is altered directly by three factors: the presence of Tregs, the presence of TGF-β, and the limitations of access to the interior of the tumor due to poor blood vessel perfusion. By calculating the killing rate with and without each of these suppressive effects in place, the relative strength of each effect can be quantified.

The tumors marked at points **A** and **B** in Fig. 2 take the same amount of time to reach 10^{11} cells but exhibit different suppression profiles. Fig. 6 shows the results of a simulation for a tumor with parameters $\gamma = 333$ and $\log a = -4.2$, corresponding to point **A**.

Fig. 6a shows the populations of tumor cells, effector T cells, and Tregs. With such low antigenicity, the number of T cells never becomes large enough to fight the tumor effectively. Fig. 6b shows how the T cell population is divided between helper cells, effector cells, and Tregs. As the tumor grows, it recruits more Tregs, primarily by producing TGF-β which converts the helper cells. The fraction of Tregs increases steadily with tumor size, as seen in clinical settings (Woo et al., 2001; Liyanage et al., 2002; Wolf et al., 2003).

Fig. 6c shows the fraction of Tregs that is naturally expanded from the memory population, and the fraction that is derived from helper cells. Fig. 6d shows the suppressive effects that are acting to prevent tumor cell killing. The solid line represents the relative tumor kill rate due to all suppressive effects, where a value of 1 would indicate that there is no suppression of the killing rate. The three other traces show the contribution to this suppression by Tregs, TGF-β, and tumor access limitation (T^*). For this growth rate and antigenicity, Tregs exert increasing suppression with increasing tumor size, but the primary reason that the tumor escapes is that the effector T cell numbers are too low to provide a significant tumor cell kill. TGF-β suppression is only significant when the tumor is large. Limited access to the interior of the tumor does not significantly affect the immune system response, because tumor-to-effector cell ratio is large, regardless of access limitations. The effector cells that are present are insufficient to battle the accessible tumor cells, regardless of access to the interior. This tumor still escapes when the TGF-β suppression is removed, as shown in Fig. 5.

By contrast, Fig. 7 shows the results of the model for a tumor with parameters $\gamma = 574$ and $\log a = 1$. This corresponds to the point labeled **B** in Fig. 2. In this case, the Tregs expand very quickly, and immediately suppress T-cell killing. T-cell numbers are very high, but limited access to the center of the tumor also limits the immune system efficacy, as seen in the suppression plot (Fig. 7d). Treg suppression is enhanced by early conversion of helper cells into Tregs. Although the high antigenicity causes large numbers of effector T cells to develop, there are also large numbers of helper T cells, which in turn become Tregs through TGF-β mediated conversion. This enhances Treg suppression of tumor cell killing. If the TGF-β suppression were removed or Treg suppression were to be reduced, this tumor would be controlled, instead of growing without bound.

In order to achieve the optimal immune response, the antigenicity has to be large enough to provoke a significant immune response, but not so large that the suppressive effects overwhelm the cytotoxic ability of effector T cells.
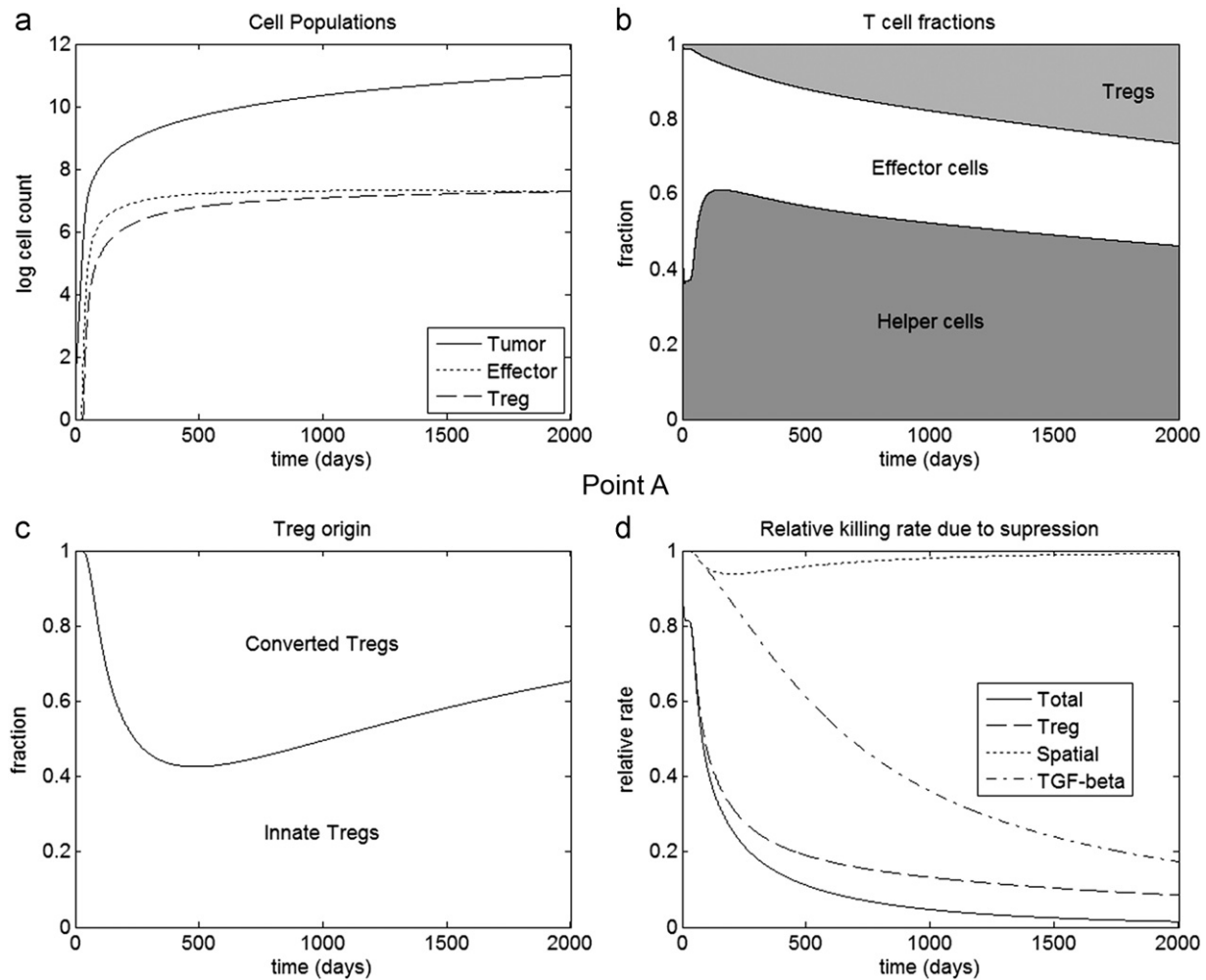
Fig. 6. Simulation of tumor growth for $\log a = -4.2$ and $\gamma = 333$, corresponding to point **A** in Fig. 2. (a) Cell populations over time, (b) T cell fractions, (c) Treg origination, and (d) suppression of tumor cell killing rate.

Tregs and TGF-β appear to have the most significant suppressive effect on tumor cell killing, consistent with experimental evidence showing the importance of these suppressive factors (Gorelik and Flavell, 2001; Viehl et al., 2006; Frumento et al., 2006; Kobie and Akporiaye, 2003; Wojtowicz-Praga, 2003), with Tregs particularly acting in the early stages of tumor growth. IL-10 had a limited qualitative effect on tumor outcomes in the model, for the production rates derived from the literature. In all cases, TGF-β does not appear to have a significant suppressive effect until the tumor is large, 10^7 cells or more. TGF-β-induced conversion of helper cells into Tregs also becomes significant primarily above this threshold.

The lack of access to the center of the tumor by the effector cells is a significant factor limiting the tumor cell killing when effector cell numbers are high. This could limit the effectiveness of adoptive immunotherapies which increase T-cell numbers and dendritic cell-based therapies which promote dendritic cell activity, since they cannot easily penetrate the tumor interior, therefore limiting the effect of additional cytotoxic cells.

5.3. Fixed point analysis

Numerical simulations using the model show the existence of fixed points, as well as stable limit cycles. These are observed within the biologically reasonable range of values for the variables, specifically tumor sizes between 1 cell and 10^8 cells.

Numerical analysis of fixed points was performed. Fixed points were found by using a root solver in Mathematica (published by Wolfram Research, Champaign, IL), and the eigenvalues of the Jacobian of the matrix of equations were examined to determine the type and stability of the fixed points.

Fig. 8 shows bifurcation diagrams for several values of the antigenicity, using the tumor growth rate as the bifurcation parameter. The vertical axis shows the number of tumor cells on a log scale. For a tumor with low antigenicity (Fig. 8a), the stable branch (solid line) and the unstable branch (dotted line) annihilate at a low growth rate. Tumors which grow slower than this value will reach the stable equilibrium branch, while tumors that grow faster will escape without bound, since the zero solution is unstable.

As the antigenicity is increased (Fig. 8b), the stable branch moves lower and becomes a stable limit cycle (dashed line) for a certain range of growth rates. Tumors in this parameter regime exhibit oscillatory behavior. It is possible that the oscillations may cause the tumor to be smaller than one cell at the minima of each cycle, therefore effectively curing the tumor, but this effect does not significantly affect the analysis of the tumor dynamics. The oscillations are small enough that the *Removal* region of Fig. 2 would be only slightly larger than shown if the oscillatory nature of these tumors were considered when determining if the tumor was cured or controlled.

A further increase in antigenicity (Fig. 8c) leads to the development of two lobes in the bifurcation diagram. Slower growing
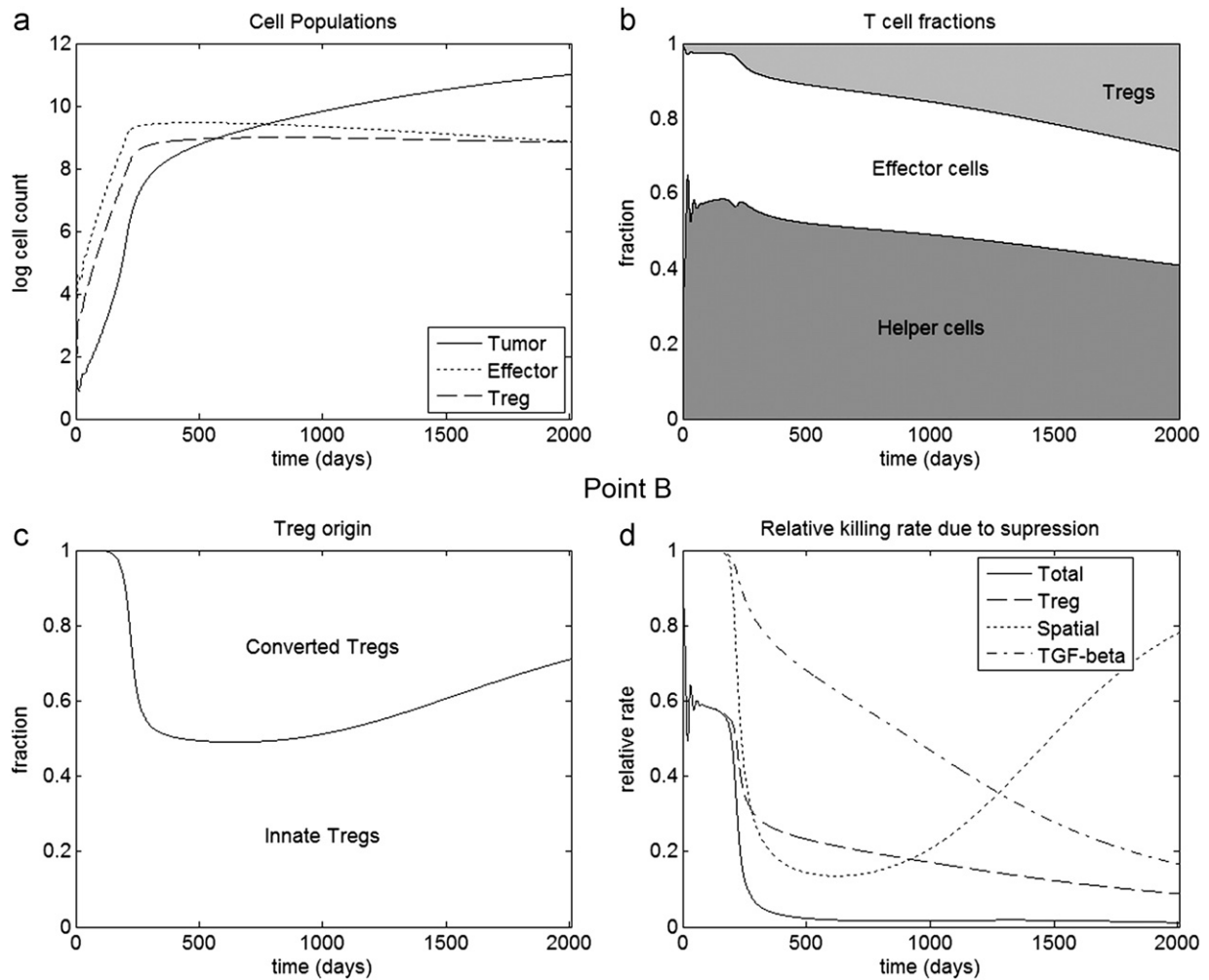
Fig. 7. Simulation of tumor growth for $\log a = 1$ and $\gamma = 574$, corresponding to point **B** in Fig. 2. (a) Cell populations over time, (b) T cell fractions, (c) Treg origination, and (d) suppression of tumor cell killing rate.

tumors will reach the lower stable branch. Tumors growing faster than the growth rate at the lower bifurcation point will reach the upper stable branch instead.

The lower branch continues to descend on the diagram with increasing antigenicity, and eventually will cross into the cure boundary of one tumor cell (Fig. 8d). Until this level antigenicity is reached, there is no mechanism for complete tumor removal by the immune system.

This behavior continues with increasing antigenicity until the upper stable lobe no longer extends beyond the lower lobe (Fig. 8e). Since the lower stable branch has moved below the cure boundary of one tumor cell, and the upper stable branch is inaccessible from an initial condition of one cell, the dynamics only allow for two options. If the growth rate is less than the lower-lobe bifurcation point (approximately $\gamma = 435$) then the tumor will be removed. If the growth rate is higher, it will grow without bound. There is no stable control of the tumor, since the fixed points are either below one cell or inaccessible to a growing tumor. Mathematically, it is of interest to note that tumors which are removed do not go to zero size in the simulation. If the condition for tumor cure were removed from the simulation, all cured tumors would reach a stable fixed point or limit cycle with values less than one cell.

Further increases in antigenicity beyond Fig. 8f do not significantly affect the dynamics. Tumors either grow without bound

or are removed by the immune system. The bifurcation point stabilizes with respect to antigenicity, as seen by the horizontal boundary between the *Removal* and *Growth* regions on the right side of Fig. 2. This phenomenon occurs because the immune system saturates at such high antigenicities, and therefore only the growth rate determines the long-term behavior of the tumor.

If the analysis is performed with different initial conditions ($T_0 = 10^5$, for example), then the upper stable branch that is inaccessible to a small tumor at high antigenicities may be reached. Although this branch does not affect the dynamics of tumor started from one cell, it may have an implication for modeling of experiments where a tumor is implanted or injected into a host. In addition, tumors are known to change phenotypes over the course of their growth due to continual mutation and selection, and therefore the dynamical path may lead to one of these stable branches due to changing parameter values over time. However, in the present work we restrict our study to tumors grown from one cell with fixed parameters.

5.4. Behavior of small tumors in the limiting case

Since a tumor behaves differently at small sizes than at large sizes, both with respect to growth law and immune system accessibility, the model can be examined in the limiting case as $T \ll T_1$, where T_1 is the transition size between growth laws.
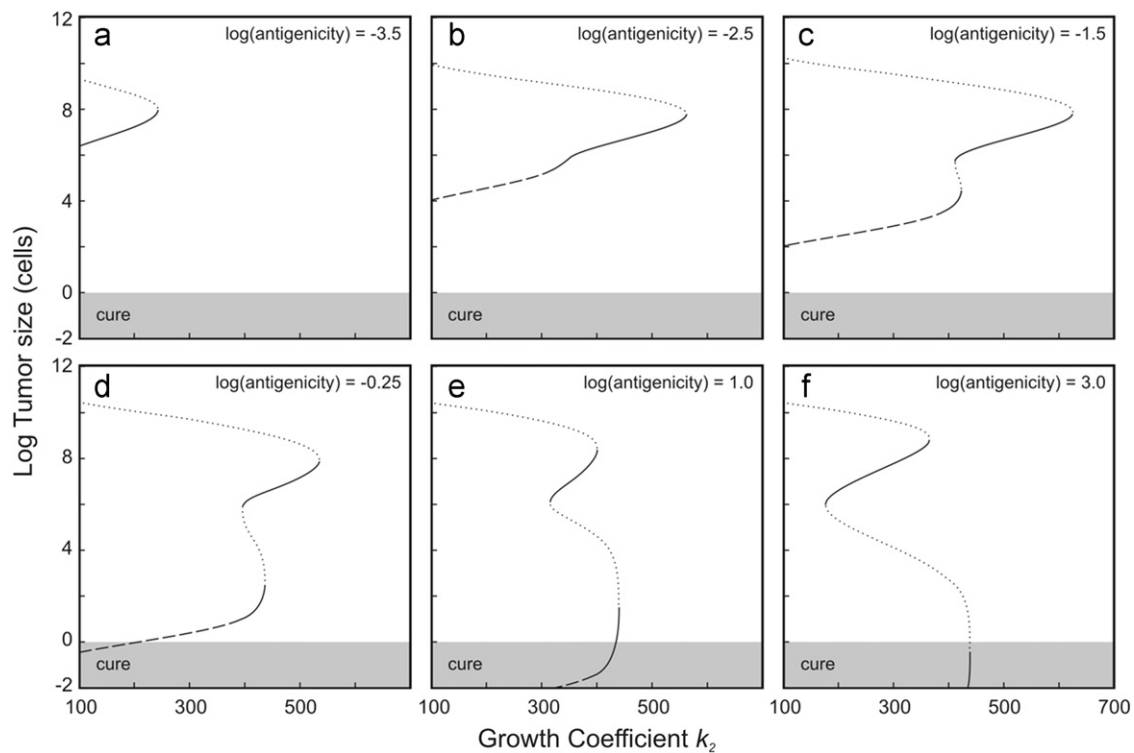
Fig. 8. Bifurcation diagrams for various antigenicities. Solid lines indicate stable fixed points, dotted lines indicate unstable fixed points, and dashed lines indicate the unstable fixed points within a stable limit cycle.

For small tumors, TGF-β production is negligible, so Eq. (18) can be written as

$$\dot{T} = \gamma_1 T - \frac{r_0 T}{(1+k_2 \frac{T}{E})} \cdot \frac{1}{(1+k_3 \frac{R}{E})}. \tag{36}$$

The fixed point of this equation occurs when $\dot{T} = 0$, or when

$$\frac{r_0}{\gamma(T_1)^{m-1}} = \left(1 + k_2 \frac{T}{E}\right)\left(1 + k_3 \frac{R}{E}\right), \tag{37}$$

where γ_1 was replaced using Eq. (30). The primary interest of modeling cancer is to find regimes where the tumor diminishes in size. For small tumors, this occurs whenever

$$\frac{r_0}{\gamma(T_1)^{m-1}} > \left(1 + k_2 \frac{T}{E}\right)\left(1 + k_3 \frac{R}{E}\right). \tag{38}$$

Since the right-hand side of Eq. (38) is always greater than 1, if the exponential growth rate $\gamma(T_1)^{m-1}$ is higher than the killing rate r_0, there is no possibility that the immune system can reduce the tumor burden. For the parameters used in this analysis given in Tables 1–4, tumors with growth rates $\gamma > 900$ will always grow to a large size.

For tumors with $\gamma < 900$, the behavior of the tumor will depend on the right-hand side of Eq. (38). A failure of the immune system to clear a tumor is either due to insufficient numbers of effector cells for a given tumor size, leading to a large value for the first term on the right-hand side, or high Treg ratios, leading to a high value for the second term. These are the two mechanisms represented respectively by points **A** and **B** in Fig. 2. The tumor with low antigenicity at point **A** escapes because of decreased T-cell stimulation, so the first term on the right side of Eq. (38) dominates. For the highly antigenic tumor at point **B**, the T/E ratio is very low, since T cells are highly stimulated by the tumor. However, the second term begins to dominate, since Tregs ratios become saturated with increased antigenicity. In between these two regimes lies the optimal region, where the right hand
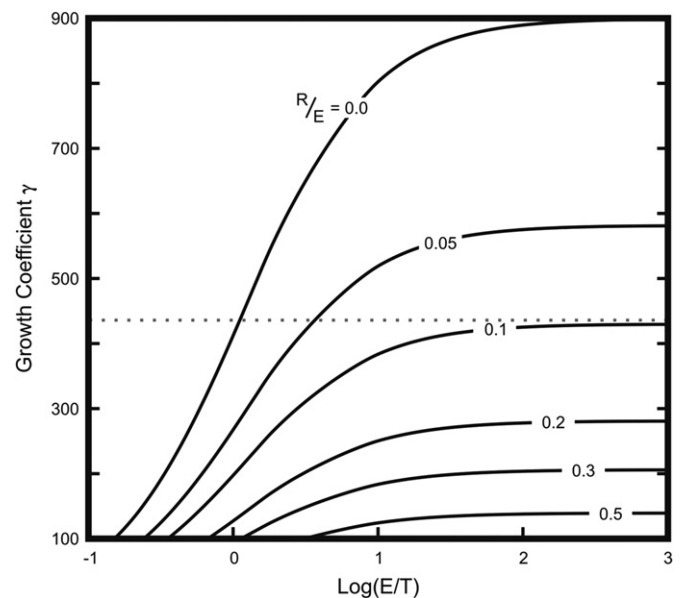

Fig. 9. Solutions of Eq. (37) for fixed values of R/E. For a given R/E ratio, combinations of $(\log(E/T), \gamma)$ that fall above the curve will lead to tumor growth, and combinations below the curve will lead to tumor removal. The curve for $R/E = 0.1$ approaches the dotted asymptote shown at $\gamma = 435$, which corresponds to the sharp upper edge of the transition from removal to growth in Fig. 2.

side of Eq. (38) is minimized, and the killing rate has the greatest advantage over the growth rate.

Fig. 9 shows solution curves of Eq. (37) assuming that the ratio R/E remains constant. For any given constant ratio R/E, a choice of the parameter γ and asymptotic ratio T/E characterizes a unique point $(\log(E/T), \gamma)$. If this point is above the corresponding curve, the dynamics of the system will lead to unbounded tumor

growth, whereas a point below the curve will lead to tumor removal.

As discussed in Section 5.1, for high antigenicities there is a sharp transition between tumors that are cured and tumors that grow to a large size, greater than $T_1 = 10^6$ cells. This is because E/T ratios are large in this regime, making the first term on the right side of Eq. (38) insignificant. The dynamic of the tumor is therefore determined by the ratio of Tregs to effector cells. For high values of antigenicity, the ratio of Tregs to effector T cells will approach 0.1, since Treg conversion from helper cells is negligible when a tumor is small. The contour for $R/E = 0.1$ in Fig. 9 approaches a γ value of about 435 for high E/T ratios (dotted line in Fig. 9). This effectively sets an upper limit for the growth rate of a tumor that can be fully removed or controlled at a small size by the immune system, and corresponds to the sharp boundary between the *Removal* and *Growth* areas on the right side of Fig. 2. It also matches the value of the lower bifurcation point in Fig. 8f.

5.5. Dendritic cell therapy

Dendritic cell therapy is performed by removing APCs from the patient, pulsing the cells with the tumor-specific peptide *in vitro*, and then inserting these cells back into the patient (Fong and Engleman, 2000). This therapy is meant to bypass the need for dendritic cells to acquire peptide from the tumor, a process which is highly suppressed by most tumors. Once the dendritic cells migrate to the lymph nodes, they can activate T cells. The number of DCs injected into a patient is between 10^6 and 10^7 cells (Brossart et al., 2000). The therapy can be administered repeatedly, and toxicity is minimal.

At the time of each treatment cycle in the simulation, the number of unlicensed dendritic cells (U) is increased by 5×10^6 cells. The schedule used in the simulations is a series of dendritic cell injections spread 14 days apart, corresponding to the treatments given in Brossart et al. (2000). Since the treatment has low toxicity, it can presumably be continued indefinitely, and in clinical trials it was terminated only when the tumor showed progressive growth.

Fig. 10 shows three cases of dendritic cell therapy for a tumor with antigenicity of $\log a = -4$. A log-scale plot shows the tumor cell count, the effector T-cell count, and the Treg cell count from just before treatment to just after. The rectangular pulses show the time points when dendritic cells were administered in the simulation. In all cases, the number of effector cells and Tregs increases after the first dose of therapy. However, the outcomes are different.

At a slow tumor growth rate of $\gamma = 150$, shown in the top panel, it would take 15 cycles of treatment to fully remove a tumor, corresponding to 7 months of therapy. This assumes that the tumor does not develop a resistance to the treatment, which is possible over that time period. Tumors which grow faster than this rate would naturally require further extensions of treatment to attain a cure. Tumors with growth rates of up to $\gamma = 350$ can be removed by continuous therapy. It is of interest to note that the interval chosen of 14 days is optimal; shortening or lengthening this interval extends the time needed to remove the tumor (not shown). This suggests that the benefits of therapy can last up to 2 weeks after treatment, which is in agreement with the timescales of T-cell expansion and decay.

If the tumor has a growth rate between $350 < \gamma < 500$, then the treatment will fail to remove the tumor, even if the cycles are administered indefinitely. The central panel of Fig. 10 shows this case, where two years of therapy are applied to a tumor with growth rate $\gamma = 370$. Indefinite treatment at these growth rates will cause the tumor to be maintained at a small size, close to 10^6
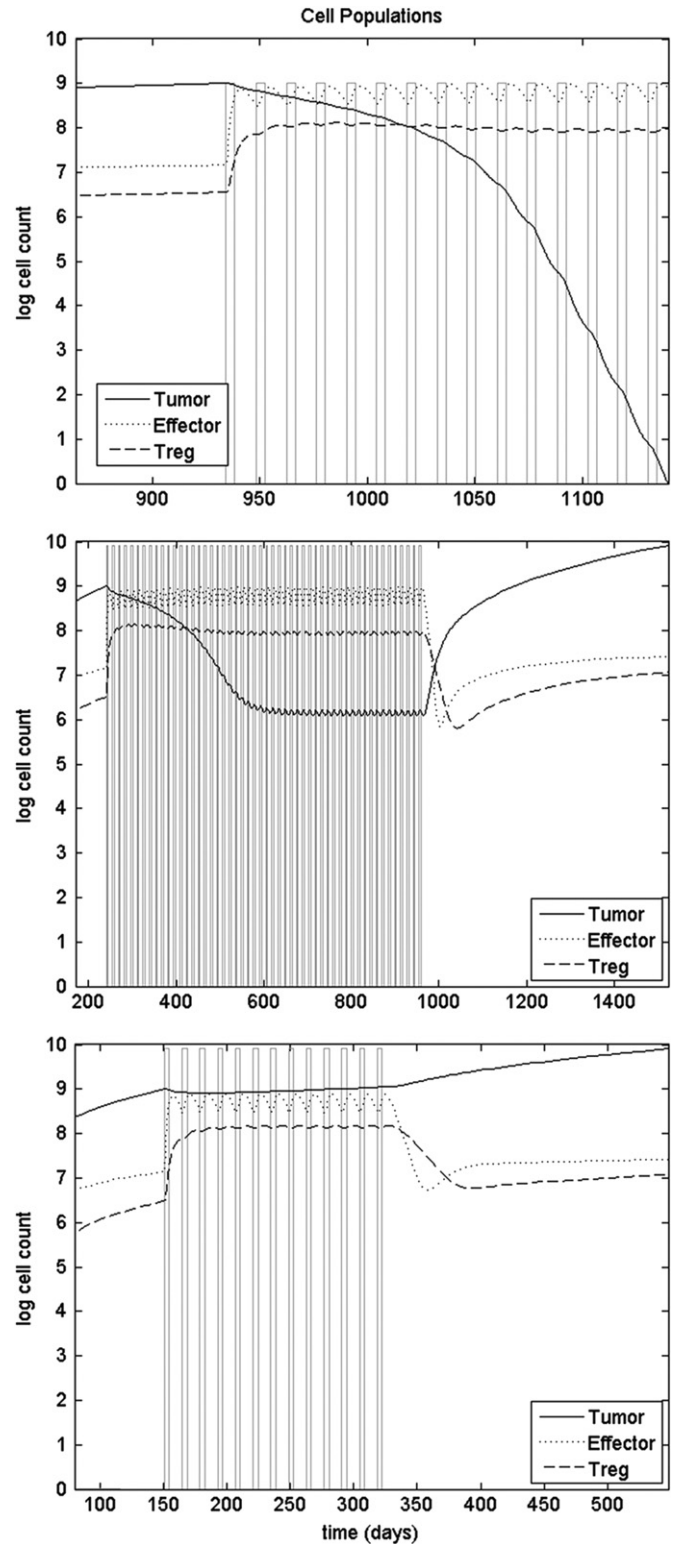

Fig. 10. The effects of dendritic cell therapy are shown for three different tumors. The rectangular pulses show the therapy intervals. The tumor growth rate is $\gamma = 150$ in the top panel, $\gamma = 370$ for the central panel, and $\gamma = 550$ for the bottom panel. Slow growing tumors can be cured with extended dendritic therapy, moderately growing tumors can be maintained at a small size as long as treatment continues; and fast growing tumors will escape the therapy regardless of treatment prolongation.

for the example shown; if the treatment is abandoned, the tumor will grow once again. It should be noted that the steady-state size may be below the level of detection, and therefore a full clinical

response maybe seen, despite persistence of a small mass of tumor cells.

Interestingly, when treatment is abandoned, the population count of the short lived effector T cells falls much quicker than the more stable Tregs, and this causes a period where Tregs outnumber effector cells, until this transient behavior is damped out. During this period, the suppression due to Tregs is very great due to the enhanced R/E ratio, and therefore effector T cell cytotoxicity is lower. This results in faster tumor growth during this period than would be normal in the absence of treatment. Although there are no known *in vivo* measurements of Treg populations following the abandonment of dendritic cell treatment, the model suggests that the transient nature of the population sizes immediately following treatment can have an effect on subsequent tumor progression. Perhaps a step-down of dendritic cell doses would be of benefit after prolonged dendritic cell therapy, to avoid an immunosuppressed period.

For growth rates greater than $\gamma = 500$, the tumor will escape treatment, regardless of how long the treatment is administered. There may be an initial period of tumor reduction from the treatment, but after a few cycles the tumor escapes and grows without bound. This case is shown in the bottom panel of Fig. 10, for a tumor with $\gamma = 550$. The first three treatments appear promising, causing a slight reduction in tumor burden. However, after the fourth treatment, the tumor begins to progress again, and further administrations of the therapy do not halt progression. The tumor progresses more slowly during the treatment as opposed to when the treatment is abandoned, but the long term outcome will be the same. The reason for the initial reduction in tumor burden is that the effector T cells react faster to the influx of DCs than the Tregs do. After a few cycles, the Tregs have caught up to the effector cells, and the immunosuppression that they cause is restored.

Changing the amount of dendritic cells has a significant effect on the outcome of treatment. Although it would seem that increased dendritic cell transfusion would always result in increased immune response, this is not the case. Fig. 11 shows the effect of varying the amount of dendritic cells transferred during therapy for a tumor with growth rate of $\gamma = 370$ and $a = 10^{-4}$. In the top panel, 10^6 dendritic cells are transferred. The tumor growth is stopped for a few cycles, but then the tumor escapes the therapy and continues to grow. In the central panel, twice as many cells (2×10^6) are administered. In this case, the tumor is gradually reduced in size with each application of therapy. If the therapy were to continue, this tumor would be removed. The bottom panel shows the results when 3×10^6 cells are administered. In this case, the tumor is reduced and maintained at a small size, but is never removed by the therapy.

This result suggests that immunotherapies may have optimal values that are not the maximum tolerated dosage. This effect could be tested in murine models if identical tumor cell lines were implanted into animals receiving different doses of dendritic cell therapy. The results also suggest that immunotherapies may be very sensitive to the conditions of the host at the time of treatment. This may be a factor in the heterogeneous response of clinical patients that receive immunotherapy treatments, and suggests that better markers of immune status may be necessary in order to optimize a particular immunotherapy.

5.6. Comparison with other models

A number of models of tumor–immune interactions have been published in the literature. The goal of the present study is to examine the effect of immunosuppression in the immune response against a tumor. Although several models have examined different individual aspects of immunosuppression, as described
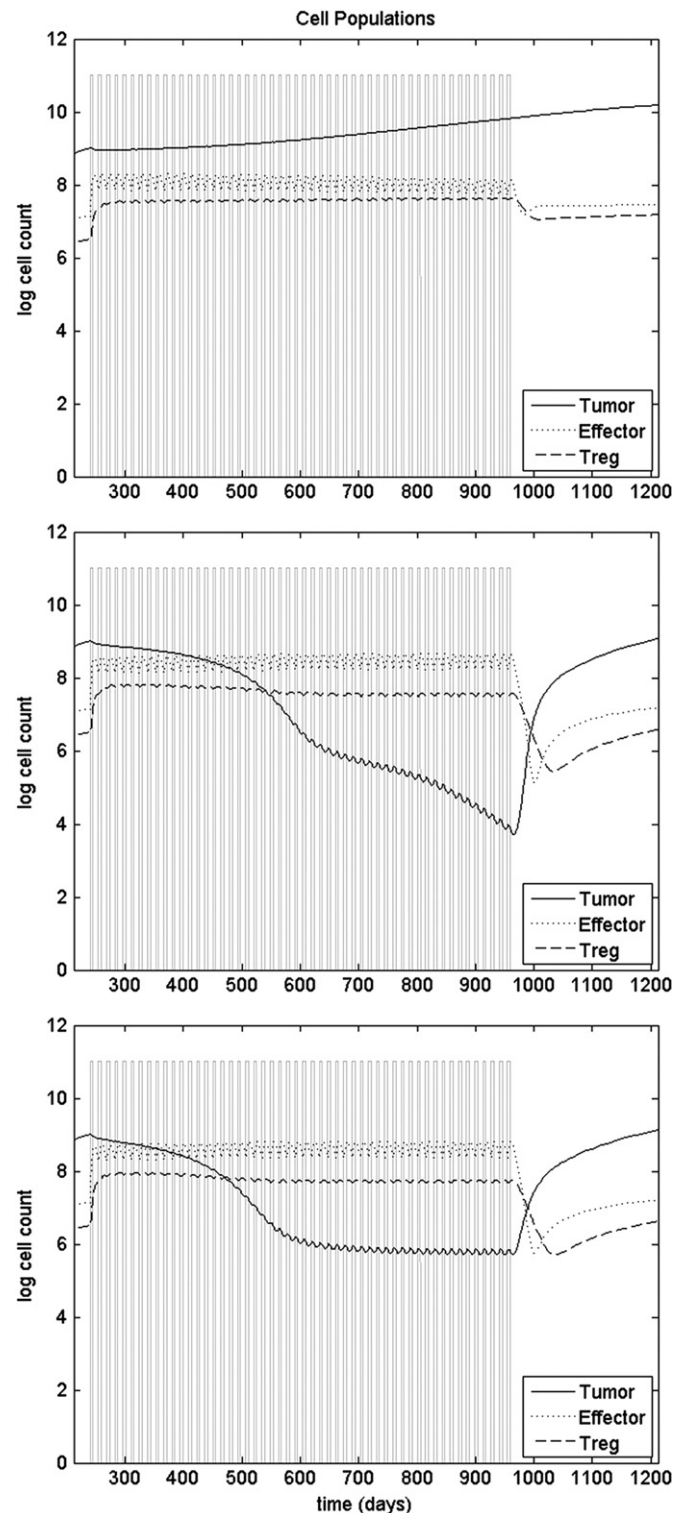

Fig. 11. The effects of dendritic cell therapy are shown for three different cell transfer amounts. The tumor growth rate is $\gamma = 370$ and the antigenicity is log $a = -4$. Therapy is administered for 2 years. 10^6 cells were administered on each dose in the top panel, 2×10^6 cells in the central panel, and 3×10^6 cells in the bottom panel. The tumor in the central panel would be cured if therapy were to continue.

below, the authors believe that the present model is a step towards understanding the interactions between multiple suppressive mechanisms, which have not been previously modeled to our knowledge. In particular, the interactions between TGF-β and Tregs have not been explicitly studied.

Arciero et al. (2004) examined the effects of TGF-β suppression on T-cell response. The mathematical model showed that tumors producing TGF-β were more likely to escape the immune system. The results of this paper are in agreement with that result, in that increased TGF-β causes increased suppression and reduced immune function. This work goes further and suggests that TGF-β primarily plays a role in fast growing, antigenic tumors, and is the main factor contributing to the existence of an optimal antigenicity, as discussed in Results section. Therefore, not only does reducing TGF-β have the potential to reduce suppression, but it also may alter the target antigenicity for therapies that attempt to modulate this parameter, such as the dendritic cell therapy presented here. By itself, the dendritic cell therapy results suggest that the system is sensitive to the numbers of cells transfused in each dose. Given the heterogeneity observed among tumors and immune cells, it is a challenge to find this optimum in a clinical setting. However, if TGF-β is reduced, the optimum antigenicity may be reduced or removed, allowing a more mono-tonic relationship between the dendritic cell dose and immune response, for example.

Leon et al. (2007) have modeled Tregs and their effect on T-cell response. The approach to Treg expansion in that study is different than the method used in the present paper, and other important suppressive elements such as TGF-β are not included. In addition, the conversion of helper T-cells into Tregs was not addressed in the Leon model. That study found two modes of unbounded tumor growth, one where the Tregs exert suppression on the effector cells, and one where the Tregs have a minimal effect. These regimes, while qualitatively corresponding to the dynamics observed for points **B** and **A**, respectively, are not distributed in the growth-antigenicity parameter space in the same way that was found in this paper. In the present work, the antigenicity of the tumor affects the immune response in a distinctly non-linear fashion, suggesting that there is an optimal antigenicity for maximal immune response. This has direct implications for some immunotherapies which have the net effect of altering the antigenicity of the system. The existence of an optimal dose for dendritic cell therapy presented here is a specific prediction which can be tested experimentally.

The model of de Pillis et al. (2005) examined T-cell interactions with natural killer cells. Multiple regimes of tumor growth, control, and removal were found. The importance of natural killer cells in that work suggests that interactions between other immune cell types have an effect on the response. However, the model did not include any suppressive effects, which were the primary focus of this work. Subsequent models by De Pillis et al. (2006, 2007) have examined the effect of treatment on the model of tumor–immune interactions. An extension of the model pre-sented here to include the effects of chemotherapy and additional immunotherapy is the subject of future work.

6. Discussion

The mathematical model developed here integrates the pri-mary suppressive mechanisms involved in the T-cell response, and quantifies the importance of the different suppressive effects at different stages of tumor growth. Regulatory T-cells appear to have a significant effect on suppression at all stages, while TGF-β has an effect that scales with tumor size. In addition, the limitations of access to the interior of a large tumor can be a significant factor in limiting the effect of the immune system. IL-10 had the least significant suppressive effect, although tumors producing high IL-10 values may exhibit different dynamics.

Tumors with different growth rates and antigenicities provoke different immune responses. Although a simple immune response model would predict that greater antigenicity would always lead to greater immune response against the tumor cells, the model presented in this work shows that there is an optimal antigenicity for fast growing tumors. If a fast-growing tumor is minimally antigenic, then there is only a small immune response; if it is highly antigenic, there may be not only a large immune response, but also a large suppressive response by Tregs and TGF-β. In between these two regimes, the immune response may be large enough to affect the tumor, but avoid excessive promotion of Tregs and other suppressive effects.

It would be of interest to expand the scope of the model to include a spatial element, and also compartmentalize the various interactions between cells. At the moment, the model simulates a well-mixed system, except for the access limitations due to vasculature already described. Since T-cell priming and expansion happens away from the tumor in the lymph nodes, this will affect the dynamics of the system. In addition, suppressive effects would be different at the tumor site than in the lymph nodes, and Treg populations in the tumor may be much greater in number than in the lymphatic system. However, estimating the parameters for these more detailed interactions presents a challenge beyond the scope of this initial model.

An additional extension that would be beneficial for under-standing T cell expansion *in vivo* would be the inclusion of the entire T cell compartment. T cell homeostasis, by which the total number of T cells is controlled in the body, is thought to play a role in the expansion rates of different T-cell types (Jameson, 2002).

Understanding the key processes in tumor–immune interac-tions will be critical to the development of effective therapies, for identification of targets, and for optimization of dosing and schedule. The model presented here takes a step towards demon-strating the effects of Tregs and TGF-β on various classes of tumors, and further extensions of the model will be used to examine how treatments interact with this system.

Acknowledgements

References

Alleva, D., Burger, C., Elgert, K., 1994. Tumor-induced regulation of suppressor macrophage nitric oxide and TNF-alpha production. Role of tumor-derived IL-10, TGF-β, and prostaglandin E2. J. Immunol. 153, 1674.

Ambrosi, D., Mollica, F., 2004. The role of stress in the growth of a multicell spheroid. J. Math. Biol. 48, 477–499.

Anderson, A., Chaplain, M., 1998. Continuous and discrete mathematical models of tumor-induced angiogenesis. Bull. Math. Biol. 60, 857–899.

von Andrian, U., Mackay, C., 2000. T-cell function and migration—two sides of the same coin. N. Engl. J. Med. 343, 1020.

Arciero, J., Jackson, T., Kirschner, D., 2004. A mathematical model of tumor–immune evasion and siRNA treatment. Discret. Contin. Dyn. Syst. Ser. B 4, 39–58.

Arstila, T., Casrouge, A., Baron, V., Even, J., Kanellopoulos, J., Kourilsky, P., 1999. A direct estimate of the human $\alpha\beta$ T cell receptor diversity. Science 286, 958.

Avradopoulos, K., Mehta, S., Blackinton, D., Wanebo, H., 1997. Interleukin-10 as a possible mediator of immunosuppressive effect in patients with squamous cell carcinoma of the head and neck. Ann. Surg. Oncol. 4, 184–190.

Boissonnas, A., Fetler, L., Zeelenberg, I., Hugues, S., Amigorena, S., 2007. *In vivo* imaging of cytotoxic T cell infiltration and elimination of a solid tumor. J. Exp. Med. 204, 345.

Boon, T., Cerottini, J., Eynde, B., Bruggen, P., Pel, A., 1994. Tumor antigens recognized by T lymphocytes. Annu. Rev. Immunol. 12, 337–365.

Breart, B., Lemaître, F., Celli, S., Bousso, P., 2008. Two-photon imaging of intratumoral CD8+ T cell cytotoxic activity during adoptive T cell therapy in mice. J. Clin. Invest. 118, 1390.

Brossart, P., Wirths, S., Stuhler, G., Reichardt, V., Kanz, L., Brugger, W., 2000. Induction of cytotoxic T-lymphocyte responses *in vivo* after vaccinations with peptide-pulsed dendritic cells. Blood 96, 3102.

Byrne, H., Preziosi, L., 2003. Modelling solid tumour growth using the theory of mixtures. Math. Med. Biol. 20, 341.

Chen, L., McGowan, P., Ashe, S., Johnston, J., Li, Y., Hellstrom, I., Hellstrom, K., 1994. Tumor immunogenicity determines the effect of B7 costimulation on T-cell mediated tumor immunity. J. Exp. Med. 179, 523.

Chouaib, S., Asselin-Paturel, C., Mami-Chouaib, F., Caignard, A., Blay, J., 1997. The host–tumor immune conflict: from immunosuppression to resistance and destruction. Immunol. Today 18, 493–497.

Curiel, T., 2007. Tregs and rethinking cancer immunotherapy. J. Clin. Invest. 117, 1167–1174.

Danforth Jr., D., Sgagias, M., 1996. Tumor necrosis factor alpha enhances secretion of transforming growth factor $\beta 2$ in MCF-7 breast cancer cells. Clin. Cancer Res. 2, 827.

De Boer, R., Perelson, A., 1994. T-cell repertoires and competitive exclusion. J. Theor. Biol. 169, 375–390.

De Pillis, L., Gu, W., Fister, K., Head, T., Maples, K., Murugan, A., Neal, T., Yoshida, K., 2007. Chemotherapy for tumors: an analysis of the dynamics and a study of quadratic and linear optimal controls. Math. Biosci. 209, 292–315.

De Pillis, L., Gu, W., Radunskaya, A., 2006. Mixed immunotherapy and chemotherapy of tumors: modeling, applications and biological interpretations. J. Theor. Biol. 238, 841–862.

Desser, L., Holomanova, D., Zavadova, E., Pavelka, K., Mohr, T., Herbacek, I., 2001. Oral therapy with proteolytic enzymes decreases excessive TGF-β levels in human blood. Cancer Chemother. Pharmacol. 47, 10–15.

Diefenbach, A., Jensen, E., Jamieson, A., Raulet, D., 2001. Rae1 and H60 ligands of the NKG2D receptor stimulate tumour immunity. Nature 413, 165–171.

Dudley, M., Wunderlich, J., Robbins, P., Yang, J., Hwu, P., Schwartzentruber, D., Topalian, S., Sherry, R., Restifo, N., Hubicki, A., et al., 2002. Cancer regression and autoimmunity in patients after clonal repopulation with antitumor lymphocytes. Science 298, 850.

Dunn, G., Bruce, A., Ikeda, H., Old, L., Schreiber, R., 2002. Cancer immunoediting: from immunosurveillance to tumor escape. Nat. Immunol. 3, 991–998.

Dunn, G., Koebel, C., Schreiber, R., 2006. Interferons, immunity and cancer immunoediting. Nat. Rev. Immunol. 6, 836–848.

Fitzpatrick, D., Bielefeldt-Ohmann, H., Himbeck, R., Jarnicki, A., Marzo, A., Robinson, B., 1996. Tumour-induced immunosuppression and autocrine growth: use of inducible anti TGF-β antisense RNA transfectants in a mesothelioma model. Lung Cancer 15, 260.

Fong, L., Engleman, E., 2000. Dendritic cells in cancer immunotherapy. Annu. Rev. Immunol. 18, 245–273.

Friberg, S., Mattson, S., 1997. On the growth rates of human malignant tumors: implications for medical decision making. J. Surg. Oncol. 65, 284–297.

Frumento, G., Piazza, T., Di Carlo, E., Ferrini, S., 2006. Targeting tumor-related immunosuppression for cancer immunotherapy. Endocr. Metab. Immune Disord. Drug Targets 6, 223–237.

Gastl, G., Abrams, J., Nanus, D., Oosterkamp, R., Silver, J., Liu, F., Chen, M., Albino, A., Bander, N., 1993. Interleukin-10 production by human carcinoma cell lines and its relationship to interleukin-6 expression. Int. J. Cancer 55, 96–101.

Gorelik, L., Flavell, R., 2001. Immune-mediated eradication of tumors through the blockade of transforming growth factor β signaling in T cells. Nat. Med. 7, 1118–1122.

Haring, J., Pewe, L., Perlman, S., 2001. High-magnitude, virus-specific CD4 T-cell response in the central nervous system of coronavirus-infected mice. J. Virol. 75, 3043.

Hart, D., Shochat, E., Agur, Z., 1998. The growth law of primary breast cancer tumors as inferred from mammography screening trials. Br. J. Cancer 78, 382–387.

Harty, J., Badovinac, V., 2008. Shaping and reshaping CD8+ T-cell memory. Nat. Rev. Immunol. 8, 107–119.

Hellstrom, K., Hellstrom, I., 1991. Principles of tumor immunity: tumor antigens. In: De Vita, V., Hellman, S., Rosenberg, S. (Eds.), Biologic Therapy of Cancer: Principles and Practices, J.B. Lippincott, Philadelphia, pp. 35–52.

Hellstrom, K., Hellstrom, I., 1974. Lymphocyte-mediated cytotoxicity and blocking serum activity to tumor antigens. Adv. Immunol. 18, 209–277.

Hsieh, C., Chen, D., Hwang, L., 2000. Tumor-induced immunosuppression: a barrier to immunotherapy of large tumors by cytokine-secreting tumor vaccine. Hum. Gene Ther. 11, 681–692.

Iwashita, I., Ueyama, T., Iwashita, A., Kawamoto, K., Kitagawa, S., Motooka, M., Utsunomiya, T., Masuda, K., 1998. Natural history of colorectal carcinoma: can the tumor volume doubling time be predicted by radiologic findings or immunohistochemical variables? J. Surg. Oncol. 68, 215.

Jackson, C., Talpos, G., Block, M., Norum, R., Lloyd, R., Tashjian, A., 1984. Clinical value of tumor doubling estimations in multiple endocrine neoplasia type II. Surgery 96, 981–987.

Jain, R., Ward-Hartley, K., 1984. Tumor blood flow: characterization, modifications, and role in hyperthermia. IEEE Trans. Sonics Ultrason. 31, 504–526.

Jameson, S., 2002. Maintaining the norm: T-cell homeostasis. Nat. Rev. Immunol. 2, 547–556.

Jarnicki, A., Lysaght, J., Todryk, S., Mills, K., 2006. Suppression of antitumor immunity by IL-10 and TGF-β-producing T cells infiltrating the growing tumor: influence of tumor environment on the induction of CD4+ and CD8+ regulatory T cells. J. Immunol. 177, 896.

Kim, H., Han, M., Do, K., Kim, K., Choi, H., Kim, A., Sung, M., Chang, K., 2002. Volume of cervical lymph nodes using 3D ultrasonography. Differentiation of metastatic from reactive lymphadenopathy in primary head and neck malignancy. Acta Radiol. 43, 571.

Kirschner, D., Panetta, J., 1998. Modeling immunotherapy of the tumor–immune interaction. J. Math. Biol. 37, 235–252.

Kobie, J., Akporiaye, E., 2003. Immunosuppressive role of transforming growth factor beta in breast cancer. Clin. Appl. Immunol. Rev. 3, 277–287.

Konrad, M., Hemstreet, G., Hersh, E., Mansell, P., Mertelsmann, R., Kolitz, J., Bradley, E., 1990. Pharmacokinetics of recombinant interleukin 2 in humans. Cancer Res. 50, 2009.

Kripke, M., 1974. Antigenicity of murine skin tumors induced by ultraviolet light. J. Natl. Cancer Inst. 53, 1333.

Kuznetsov, V., Makalkin, I., Taylor, M., Perelson, A., 1994. Nonlinear dynamics of immunogenic tumors: parameter estimation and global bifurcation analysis. Bull. Math. Biol. 56, 295–321.

Larmonier, N., Marron, M., Zeng, Y., Cantrell, J., Romanoski, A., Sepassi, M., Thompson, S., Chen, X., Andreansky, S., Katsanis, E., 2007. Tumor-derived CD4+ CD25+ regulatory T-cell suppression of dendritic cell function involves TGF-β and IL-10. Cancer Immunol. Immunother. 56, 48–59.

Le, T., Leung, L., Carroll, W., Schibler, K., 1997. Regulation of interleukin-10 gene expression: possible mechanisms accounting for its upregulation and for maturational differences in its expression by blood mononuclear cells. Blood 89, 4112.

Leon, K., Garcia, K., Carneiro, J., Lage, A., 2007. How regulatory CD25+ CD4+ T cells impinge on tumor immunobiology? On the existence of two alternative dynamical classes of tumors. J. Theor. Biol. 247, 122–137.

Liu, K., Waskow, C., Liu, X., Yao, K., Hoh, J., Nussenzweig, M., 2007a. Origin of dendritic cells in peripheral lymphoid organs of mice. Nat. Immunol. 8, 578–583.

Liu, V., Wong, L., Jang, T., Shah, A., Park, I., Yang, X., Zhang, Q., Lonning, S., Teicher, B., Lee, C., 2007b. Tumor evasion of the immune system by converting CD4+ CD25− T cells into CD4+ CD25+ T regulatory cells: role of tumor-derived TGF-β. J. Immunol. 178, 2883.

Liyanage, U., Moore, T., Joo, H., Tanaka, Y., Herrmann, V., Doherty, G., Drebin, J., Strasberg, S., Eberlein, T., Goedegebuure, P., et al., 2002. Prevalence of regulatory T cells is increased in peripheral blood and tumor microenvironment of patients with pancreas or breast adenocarcinoma. J. Immunol. 169, 2756.

Lotze, M., Frana, L., Sharrow, S., Robb, R., Rosenberg, S., 1985. In vivo administration of purified human interleukin 2. I. Half-life and immunologic effects of the Jurkat cell line-derived interleukin 2. J. Immunol. 134, 157.

McKarns, S., Schwartz, R., 2005. Distinct effects of TGF-$\beta 1$ on CD4+ and CD8+ T-cell survival, division, and IL-2 production: a role for T-cell intrinsic Smad3. J. Immunol. 174, 2071.

Mempel, T., Henrickson, S., Von Andrian, U., 2004. T-cell priming by dendritic cells in lymph nodes occurs in three distinct phases. Nature 427, 154–159.

Norton, L., 1988. A Gompertzian model of human breast cancer growth. Cancer Res. 48, 7067–7071.

Peer, P., Van Dijck, J., Verbeek, A., Hendriks, J., Holland, R., 1993. Age-dependent growth rate of primary breast cancer. CA Cancer J. Clin. 71, 3547–3551.

Piccirillo, C., Shevach, E., 2001. Cutting edge: control of CD8+ T cell activation by CD4+ CD25+ immunoregulatory cells. J. Immunol. 167, 1137.

de Pillis, L., Radunskaya, A., Wiseman, C., 2005. A validated mathematical model of cell-mediated immune response to tumor growth. Cancer Res. 65, 7950.

Roitt, I., Delves, P., 2001. Roitt's Essential Immunology. Blackwell Science Inc., Oxford.

Romani, N., Inaba, K., Puré, E., Crowley, M., Witmer-Pack, M., Steinman, R., 1989. A small number of anti-CD3 molecules on dendritic cells stimulate DNA synthesis in mouse T lymphocytes. J. Exp. Med. 169, 1153.

Roose, T., Chapman, S., Maini, P., 2007. Mathematical models of avascular tumor growth. SIAM Rev. 49, 179–208.

Rosenberg, S., Lotze, M., 1986. Cancer immunotherapy using interleukin-2 and interleukin-2-activated lymphocytes. Annu. Rev. Immunol. 4, 681–709.

Rosenberg, S., Spiess, P., Lafreniere, R., 1986. A new approach to the adoptive immunotherapy of cancer with tumor-infiltrating lymphocytes. Science 233, 1318.

Seddiki, N., Santner-Nanan, B., Tangye, S., Alexander, S., Solomon, M., Lee, S., Nanan, R., de Saint Groth, B., 2006. Persistence of naive CD45RA+ regulatory T cells in adult life. Blood 107, 2830.

Setoguchi, R., Hori, S., Takahashi, T., Sakaguchi, S., 2005. Homeostatic maintenance of natural Foxp3+ CD25+ CD4+ regulatory T cells by interleukin (IL)-2 and induction of autoimmune disease by IL-2 neutralization. J. Exp. Med. 201, 723.

Skipper, H., 1971. Kinetics of mammary tumor cell growth and implications for therapy. Cancer 28, 1479–1499.

Skog, A., Wadhwa, M., Hassan, M., Gharizadeh, B., Bird, C., Ragnhammar, P., Thorpe, R., Mellstedt, H., 2001. Alteration of interleukin 2 (IL-2) pharmacokinetics and function by IL-2 antibodies induced after treatment of colorectal carcinoma patients with a combination of monoclonal antibody 17-1A, granulocyte macrophage colony-stimulating factor, and IL-2. Clin. Cancer Res. 7, 1163.

Smith, C., Wilson, N., Waithman, J., Villadangos, J., Carbone, F., Heath, W., Belz, G., 2004. Cognate CD4^{+} T cell licensing of dendritic cells in CD8^{+} T-cell immunity. Nat. Immunol. 5, 1143–1148.

Steele, G., 1977. Growth Kinetics of Tumors. Clarendon, Oxford.

Taga, K., Mostowski, H., Tosato, G., 1993. Human interleukin-10 can directly inhibit T-cell growth. Blood 81, 2964.

Tannock, I., Lee, C., Tunggal, J., Cowan, D., Egorin, M., 2002. Limited penetration of anticancer drugs through tumor tissue. Clin. Cancer Res. 8, 878.

Taylor, J., Fahey, J., Detels, R., Giorgi, J., 1989. CD4 percentage, CD4 number, and CD4:CD8 ratio in HIV infection: which to choose and how to use. J. Acquired Immune Defic. Syndr. 2, 114.

Thomas, D., Massagué, J., 2005. TGF-β directly targets cytotoxic T-cell functions during tumor evasion of immune surveillance. Cancer Cell 8, 369–380.

Vaage, J., 1971. Concomitant immunity and specific depression of immunity by residual or reinjected syngeneic tumor tissue. Cancer Res. 31, 1655.

Viehl, C., Moore, T., Liyanage, U., Frey, D., Ehlers, J., Eberlein, T., Goedegebuure, P., Linehan, D., 2006. Depletion of CD4^{+} CD25^{+} regulatory T cells promotes a tumor-specific immune response in pancreas cancer-bearing mice. Ann. Surg. Oncol. 13, 1252–1258.

Villunger, A., Strasser, A., 1999. The great escape: is immune evasion required for tumor progression? Nat. Med. 5, 874–875.

Vukmanovic-Stejic, M., Zhang, Y., Cook, J., Fletcher, J., McQuaid, A., Masters, J., Rustin, M., Taams, L., Beverley, P., Macallan, D., et al., 2006. Human CD4^{+} CD25^{hi} Foxp3 regulatory T cells are derived by rapid turnover of memory populations in vivo. J. Clin. Invest. 116, 2423–2433.

de Waal Malefyt, R., Yssel, H., De Vries, J., 1993. Direct effects of IL-10 on subsets of human CD4^{+} T cell clones and resting T cells. Specific inhibition of IL-2 production and proliferation. J. Immunol. 150, 4754.

Wakefield, L., Winokur, T., Hollands, R., Christopherson, K., Levinson, A., Sporn, M., 1990. Recombinant latent transforming growth factor β1 has a longer plasma half-life in rats than active transforming growth factor β1, and a different tissue distribution. J. Clin. Invest. 86, 1976.

Waterhouse, N., Sutton, V., Sedelies, K., Ciccone, A., Jenkins, M., Turner, S., Bird, P., Trapani, J., 2006. Cytotoxic T lymphocyte-induced killing in the absence of granzymes A and B is unique and distinct from both apoptosis and perforin-dependent lysis. J. Cell Biol. 173, 133.

Wimmer, C., Rentsch, M., Crispin, A., Illner, W., Arbogast, H., Graeb, C., Jauch, K., Guba, M., 2007. The janus face of immunosuppression—de novo malignancy after renal transplantation: the experience of the Transplantation Center Munich. Kidney Int. 71, 1271–1278.

Wojtowicz-Praga, S., 2003. Reversal of tumor-induced immunosuppression by TGF-β inhibitors. Invest. New Drugs 21, 21–32.

Wolf, A., Wolf, D., Steurer, M., Gastl, G., Gunsilius, E., Grubeck-Loebenstein, B., 2003. Increase of regulatory T cells in the peripheral blood of cancer patients. Clin. Cancer Res. 9, 606.

Woo, E., Chu, C., Goletz, T., Schlienger, K., Yeh, H., Coukos, G., Rubin, S., Kaiser, L., June, C., 2001. Regulatory CD4^{+} CD25^{+} T cells in tumors from patients with early-stage non-small cell lung cancer and late-stage ovarian cancer. Cancer Res. 61, 4766.

Yates, A., Callard, R., 2001. Cell death and the maintenance of immunological memory. Discret. Contin. Dyn. Syst. 1, 43–59.